HHS Public Access

Author manuscript

*Toxicol Appl Pharmacol*. Author manuscript; available in PMC 2021 October 15.

Published in final edited form as:

*Toxicol Appl Pharmacol*. 2020 October 15; 405: 115205. doi:10.1016/j.taap.2020.115205.

# Triclosan Disrupts Immune Cell Function by Depressing $Ca^{2+}$ Influx Following Acidification of the Cytoplasm

**Suraj Sangroula**[1], **Alan Y. Baez Vasquez**[1], **Prakash Raut**[2], **Bright Obeng**[1], **Juyoung K. Shim**[4], **Grace D. Bagley**[1], **Bailey E. West**[1], **John E. Burnell**[1], **Marissa S. Kinney**[1], **Christian M. Potts**[1], **Sasha R. Weller**[1,3], **Joshua B. Kelley**[1,3], **Samuel T. Hess**[2,3], **Julie A. Gosse**[1,3,*]

[1]Department of Molecular and Biomedical Sciences, University of Maine, Orono, ME, USA

[2]Department of Physics and Astronomy, University of Maine, Orono, ME, USA

[3]Graduate School of Biomedical Science and Engineering, University of Maine, Orono, ME, USA

[4]Department of Biology, University of Maine at Augusta, Augusta, ME, USA

## Abstract

Triclosan (TCS) is an antimicrobial agent that was effectively banned by the FDA from hand soaps in 2016, hospital soaps in 2017, and hand sanitizers in 2019; however, TCS can still be found in a few products. At consumer-relevant, non-cytotoxic doses, TCS inhibits the functions of both mitochondria and mast cells, a ubiquitous cell type. Via the store-operated $Ca^{2+}$ entry mechanism utilized by many immune cells, mast cells undergo antigen-stimulated $Ca^{2+}$ influx into the cytosol, for proper function. Previous work showed that TCS inhibits $Ca^{2+}$ dynamics in mast cells, and here we show that TCS also inhibits $Ca^{2+}$ mobilization in human Jurkat T cells. However, the biochemical mechanism behind the $Ca^{2+}$ dampening has yet to be elucidated. Three-dimensional

*Corresponding author: Julie A. Gosse, Department of Molecular and Biomedical Sciences, University of Maine, Orono, ME 04469, USA. Tel. +1 207 581 4833, Julie.gosse@maine.edu.

**Suraj Sangroula**: Conceptualization, Methodology, Software, Validation, Formal analysis, Investigation, Resources, Data Curation, Writing - Original Draft, Writing - Review & Editing, Visualization
**Alan Y. Baez Vasquez**: Conceptualization, Methodology, Validation, Formal analysis, Investigation, Writing - Original Draft, Visualization, Funding acquisition
**Prakash Raut**: Conceptualization, Software, Formal analysis, Investigation, Resources, Data Curation, Writing - Original Draft
**Bright Obeng**: Validation, Formal analysis, Investigation, Writing - Original Draft, Visualization
**Juyoung K. Shim**: Methodology, Investigation, Writing - Review & Editing, Supervision
**Grace D. Bagley**: Methodology, Formal analysis, Investigation, Funding acquisition
**Bailey E. West**: Validation, Formal analysis, Investigation, Funding acquisition
**John E. Burnell**: Validation, Formal analysis
**Marissa S. Kinney**: Investigation
**Christian M. Potts**: Validation, Investigation, Writing - Review & Editing
**Sasha R. Weller**: Validation, Investigation
**Joshua B. Kelley**: Methodology, Software, Resources, Supervision
**Samuel T. Hess**: Methodology, Software, Resources, Writing - Review & Editing, Supervision, Funding acquisition
**Julie A. Gosse**: Conceptualization, Methodology, Validation, Formal analysis, Resources, Writing - Original Draft, Writing - Review & Editing, Visualization, Supervision, Project administration, Funding acquisition

Declaration of interests

The authors declare that they have no known competing financial interests or personal relationships that could have appeared to influence the work reported in this paper.

super-resolution microscopy reveals that TCS induces mitochondrial swelling, in line with and extending the previous finding of TCS inhibition of mitochondrial membrane potential via its proton ionophoric activity. Inhibition of plasma membrane potential (PMP) by the canonical depolarizer gramicidin can inhibit mast cell function. However, use of the genetically encoded voltage indicators (GEVIs) ArcLight (pH-sensitive) and ASAP2 (pH-insensitive), indicates that TCS does not disrupt PMP. In conjunction with data from a plasma membrane-localized, pH-sensitive reporter, these results indicate that TCS, instead, induces cytosolic acidification in mast cells and T cells. Acidification of the cytosol likely inhibits $Ca^{2+}$ influx by uncoupling the STIM1/ORAI1 interaction that is required for opening of plasma membrane $Ca^{2+}$ channels. These results provide a mechanistic explanation of TCS disruption of $Ca^{2+}$ influx and, thus, of immune cell function.

**Keywords**

triclosan; store-operated calcium entry; mast cell; T cell; acidification; genetically encoded voltage indicator; super-resolution microscopy

## Introduction

Triclosan (TCS) is a formerly widespread antimicrobial agent: it was estimated that 75% of the US population in 2008 was exposed to TCS (Calafat *et al.*, 2008). Recently, the U.S. Food and Drug Administration effectively banned TCS from hand soaps in 2016 (Kux, 2016), from hospital products in 2017 (Kux, 2017), and from over-the-counter hand sanitizers in 2019 (Gottlieb, 2019). TCS was also removed by the Colgate-Palmolive company from its top-selling toothpaste product (Kary, 2019) in 2019. Despite these stoppages, TCS remains in some antibacterial household products that are not regulated by the FDA and in a few remaining personal care products (www.ewg.org). TCS is readily absorbed into the skin (Queckenberg *et al.*, 2010) and oral mucosa (Gilbert, 1987) where it remains for a significant time prior to metabolism and clearance (Moss *et al.*, 2000), thus allowing for a constant chronic exposure upon periodic re-exposure. In this study, non-cytotoxic, micromolar TCS doses, that model human exposure levels to TCS following personal care product application (Weatherly and Gosse, 2017; Weatherly *et al.*, 2018), are utilized. Added to consumer products for its antimicrobial properties, TCS, ironically, inhibits the functioning of mammalian immune cells whose physiological purpose is to fight microbial infections (Udoji *et al.*, 2010; Palmer *et al.*, 2012; Hurd-Brown *et al.*, 2013).

Clinically, TCS is used for its antimicrobial (Daoud *et al.*, 2014) and anti-gingivitis properties (Rover and Leu-Wai-See, 2014). Additionally, previous studies provided evidence that TCS could potentially be used to treat atopic dermatitis (Sporik and Kemp, 1997; Tan *et al.*, 2010). Despite these positive clinical effects, within the past few years a panoply of triclosan epidemiology studies have emerged, reporting various adverse TCS health effects (Weatherly and Gosse, 2017). Adverse TCS-linked effects on the reproductive system include increased spontaneous abortion rate (Wang *et al.*, 2015), abnormal sperm morphology (Jurewicz *et al.*, 2018; Zamkowska *et al.*, 2018), and decreased fecundity (Vélez *et al.*, 2015; Zhu *et al.*, 2019). Additionally, newborn infants' weight, length, and head

circumference decreased due to TCS exposure (Etzel *et al.*, 2017). Cognitive effects have also been observed; TCS has been linked to lower cognitive test scores in children (Jackson-Browne *et al.*, 2018) and to higher behavior problem scores in 8-year old boys (Jackson-Browne *et al.*, 2019). TCS causes metabolic effects including decreased BMI (Li et al., 2015), increased risk of gestational diabetes (Ouyang *et al.*, 2018), changes in thyroid hormone levels in blood (Koeppe *et al.*, 2013; Wang *et al.*, 2017) and increased risk of type 2 diabetes in women (Xie *et al.*, 2020). Triclosan exposure is also associated with decreased bone mass density and increased osteoporosis (Cai *et al.*, 2019). Additionally, allergic rhinitis has been associated with TCS exposure (Kim and Kim, 2019). However, the cellular and molecular mechanisms underlying these epidemiological observations are not fully understood. Triclosan inhibition of mast cells (Palmer *et al.*, 2012; Weatherly *et al.*, 2013) and mitochondria (Ajao *et al.*, 2015; Shim *et al.*, 2016; Weatherly *et al.*, 2016; Weatherly *et al.*, 2018; Weatherly *et al.*, 2020), in human cells (Weatherly *et al.*, 2016) and in other species, may be related to these human health effects.

One of the underlying mechanisms of adverse human health effects caused by TCS may be its mitochondrial toxicity. An uncoupler due to its ionizable proton (Ajao *et al.*, 2015; Weatherly *et al.*, 2016), triclosan inhibits adenosine triphosphate (ATP) production and increases oxygen consumption rate in multiple cell types (Weatherly *et al.*, 2016) and in live zebrafish (Shim *et al.*, 2016). Additionally, TCS deflates mitochondrial membrane potential (MMP), thwarts mitochondrial translocation and $Ca^{2+}$ dynamics, and induces mitochondrial fission and deformation (as assessed in two-dimensional [2D], super-resolution, live-cell microscopy (Weatherly *et al.*, 2018). These TCS effects on MMP and mitochondrial morphology have been recapitulated in an *in vivo* mouse study (Weatherly *et al.*, 2020). Critically, mitochondrial toxicity by TCS has been directly connected to its instigation of inflammation and immunotoxicity: TCS increases Drp1 and decreases Opa1 expression levels, effects which both increase mitochondrial fission and activate the NLRP3 inflammasome (Weatherly *et al.*, 2020).

Separate from its mitochondrial toxicity, TCS disrupts other cellular signal transduction processes, such as $Ca^{2+}$ mobilization and cytoskeletal remodeling, which are shared by numerous cell types (Weatherly *et al.*, 2018). For example, TCS disrupts the functioning of the immunological/neurological cell type mast cells. TCS mitotoxicity explains an estimated ~10% this inhibition (Weatherly *et al.*, 2018); the complete biochemical mechanism underlying TCS inhibition of mast cell function remains unknown and is explored further in this manuscript. Mast cells are found in a large variety of tissues (Dvorak, 1986; Theoharides and Sant, 1991; Farrell *et al.*, 1995; Blank *et al.*, 2007) and are involved in defense against parasites (Metcalfe *et al.*, 1997), bacteria (Johnzon *et al.*, 2016), and cancer (Hempel *et al.*, 2017). Mast cell dysfunction is associated with neurological diseases (Silver and Curley, 2013; Girolamo *et al.*, 2017) such as multiple sclerosis (Elieh-Ali-Komi and Cao, 2017). Of course, mast cells are also major effector cells of allergy and asthma (Galli *et al.*, 2005), and previous clinical reports of atopic disorder alleviation by TCS, noted above (Sporik and Kemp, 1997; Tan *et al.*, 2010), align with our findings of mast cell inhibition by TCS (Palmer *et al.*, 2012).

Mast cells undergo degranulation, the release of bioactive mediators such as histamine and serotonin, in a process that begins with multivalent antigen (Ag) mediated cross-linking of immunoglobulin E (IgE)-primed FcεRI receptors on the cell surface. This binding initiates a phosphorylation cascade in which phospholipase C gamma (PLCγ) is activated (Kinet, 1999). PLCγ subsequently cleaves phosphatidylinositol 4,5-bisphosphate ($PIP_2$) into diacylglycerol (DAG) and phosphatidylinositol 4,5-bisphosphate ($IP_3$). The latter is then able to bind to its receptor on the endoplasmic reticulum (ER) membrane and initiate the release of ER $Ca^{2+}$ stores into the cytosol (Berridge, 1993). Reduced ER $Ca^{2+}$ concentration results in altered conformation of ER protein STIM1, causing it to bind to and change the conformation of the ORAI1 subunit of the $Ca^{2+}$ release-activated $Ca^{2+}$ (CRAC) channel, opening it to a flood of external $Ca^{2+}$ flowing into the cytosol (Vig *et al.*, 2006; Hogan *et al.*, 2010); this process is termed store-operated $Ca^{2+}$ entry, or SOCE (Putney, 1986). SOCE is required for mast cell degranulation (as reviewed in (Holowka *et al.*, 2012) because increased cytosolic $Ca^{2+}$ levels allow for events required for the movement of granules to the plasma membrane for exocytosis, such as protein kinase C (PKC) activation (Ozawa *et al.*, 1993), phospholipase D (PLD) activation (Chahdi *et al.*, 2002), and microtubule polymerization (Guo *et al.*, 1998; Smith *et al.*, 2003).

These signaling processes are important in a variety of cell types, including in the immune system and brain. SOCE mechanisms are largely conserved across cell types (Prakriya and Lewis, 2015). For example, T-cell signaling (Marano *et al.*, 1993; Trebak and Kinet, 2019) also begins with T-cell receptor (TCR) cross-linking, as with FcεRI. In T-cells (part of the adaptive immune system) *in vivo*, this crosslinking is primarily done by an antigen presenting cell (APCs; innate immune cells such as macrophage or a dendritic cells), presenting antigen on the major histocompatibility complex (Punt *et al.*, 2019). The TCR/APC interaction can be emulated *in vitro* through the use of an anti-TCR antibody (Marano *et al.*, 1993). Such cross-linking leads to PLCγ activation and subsequent generation of $IP_3$ and SOCE, via the same process outlined above for mast cells. The subsequent increase in cytosolic $Ca^{2+}$ concentration allows for calmodulin/calcineurin binding and subsequent activation of the nuclear factor of activated T-cells (Punt *et al.*, 2019; Trebak and Kinet, 2019), an important $Ca^{2+}$-dependent transcription factor. Thus, signaling upstream of SOCE is very similar between mast cells and T-cells; whereas signaling downstream of SOCE is largely different between mast cells and T-cells. While TCS is known to interfere with bodily distribution of T cells (Anderson *et al.*, 2016), cytokine production (Barros *et al.*, 2010; Marshall *et al.*, 2015; Anderson *et al.*, 2016; Marshall *et al.*, 2017), and expression of calcium-binding biomarkers of inflammation (Marshall *et al.*, 2017), triclosan effects on intracellular signal transduction, functional outcomes, and SOCE within T cells have not yet been examined.

Triclosan disrupts mast cell function by strongly inhibiting Ag-stimulated $Ca^{2+}$ influx into the cytosol via the CRAC channels (Weatherly *et al.*, 2018). This depressed cytosolic $Ca^{2+}$ concentration leads, as expected, to inhibition of downstream events, such as reduced PLD activity (Shim *et al.*, 2019) and microtubule polymerization (Weatherly *et al.*, 2018). Thus, inhibition of SOCE by TCS explains its inhibition of mast cell function. The question remains: how does TCS inhibit $Ca^{2+}$ entry through CRAC channels?

One explanation could be TCS disruption of any of the upstream signaling events leading to SOCE: FcεRI crosslinking, any link in the phosphorylation cascade, $PIP_2$ signaling function, or $IP_3$ binding to its ER membrane receptor. However, TCS does not hinder $Ca^{2+}$ efflux from the ER (Weatherly *et al.*, 2018) and does not seriously interfere with $PIP_2$ (Shim *et al.*, 2019) — evidence that TCS does not inhibit any of these events upstream of ER $Ca^{2+}$ release.

Because TCS does not hamper the signaling events culminating in ER $Ca^{2+}$ release, an alternative mechanism underlies TCS inhibition of CRAC channel $Ca^{2+}$ entry. Chemical depolarization of plasma membrane potential (PMP) reduces $Ca^{2+}$ entry into the cytosol of mast cells (Mohr and Fewtrell, 1987a) and also of T cells (Sarkadi *et al.*, 1990). Integrity of PMP is important for SOCE due to its contribution to the free energy, $\Delta G_{transport}$, available to import $Ca^{2+}$ down its electrochemical gradient into the cytoplasm. In this study, we hypothesized that TCS, as a proton ionophore (Weatherly *et al.*, 2016), inhibits $Ca^{2+}$ influx by depolarizing PMP similarly to how TCS deflates membrane potential of mitochondria (Weatherly *et al.*, 2018) and of artificial bilayers (Popova *et al.*, 2018)—by acting as a "Trojan horse" to provide safe passage for protons through lipid membranes.

The driving force for $Ca^{2+}$ influx through the CRAC channel is calculated as (Nelson and Cox, 2017)

$$\Delta G_{Transport} = RTln\left(\frac{C_2}{C_1}\right) + nZF\Delta\Psi$$

Using physiological temperature of 310K, the gas and Faraday's constants, the number of charges on the transported ion (n=2), the sign of the charge of the transported ion (Z=+), resting PMP $\Delta\Psi$ of −82.5 mV (Lindau and Fernandez, 1986; Wischmeyer *et al.*, 1995), $C_1$ = extracellular $Ca^{2+}$ concentration in the buffer (1.8 mM), and $C_2$ = average cytosolic $Ca^{2+}$ concentration in an Ag-stimulated mast cell (1 μM) (Millard *et al.*, 1988; Chandra *et al.*, 1994), the driving force (Gibbs free energy) for $Ca^{2+}$ influx through open CRAC channels is the highly exergonic value −35 kJ/mol. If TCS were to completely depolarize the mast cell PMP, the term $nZF\Delta\Psi$ would collapse to zero, the driving force behind SOCE would be reduced ~45%, to −19 kJ/mol, and, hence, 45% less $Ca^{2+}$ would flood into the cell. In fact, this PMP-knockout-predicted ~45% reduction in integrated $Ca^{2+}$ influx was observed in mast cells following 20 μM TCS exposure (Weatherly *et al.*, 2018).

Thus, in this study, the first aim was to measure TCS effects on PMP in mast cells. The mast cell model rat basophilic leukemia, clone 2H3 (RBL), which are functionally similar to mature human mast cells, rodent mucosal mast cells, and basophils (Fewtrell *et al.*, 1979; Metzger *et al.*, 1982; Seldin *et al.*, 1985; Metcalfe *et al.*, 1997; Abramson and Pecht, 2007; Lee *et al.*, 2012), was used. RBL cells are effective for toxicological studies due to their ability to respond to exogenous agents in a similar fashion as primary bone-marrow derived mast cells (Zaitsu *et al.*, 2007; Thrasher *et al.*, 2013; Alsaleh *et al.*, 2016).

Conventionally, PMP is measured through the use of patch clamping or of voltage-sensitive fluorescent organic dyes. However, traditional patch clamping is a low-throughout process. Also, TCS is a chemical quencher of many unprotected fluorescent chromophores (such as

those found in organic voltage sensitive dyes) (Weatherly, 2017). Thus, genetically encoded voltage indicators (GEVIs), reporter protein constructs with a β-barrel protein structure that protects the internal fluorophore from TCS fluorescence interference (Weatherly, 2017; Weatherly *et al.*, 2018) were used. Targeted to the plasma membrane, GEVIs communicate changes in PMP through changes in fluorescence intensity. To our knowledge, this study represents the first use of a GEVI in an immune cell model or in the field of toxicology.

An additional novel use of a biophysical technique in toxicology, three-dimensional (3D) Fluorescence Photoactivation Localization Microscopy (FPALM) super-resolution microscopy was also employed to detail TCS effects, via membrane depolarization, on mitochondrial morphology in mast cells (Parent and Hess, 2019). Conventional light microscopy, including widefield and confocal imaging, cannot resolve objects that are less than ~250 nm apart, due to the diffraction limit, but FPALM breaks this diffraction limit (Hess *et al.*, 2006). These 3D studies augment, by providing information on mitochondrial volume and surface area, previous 2D work showing that TCS disrupts mitochondrial nanostructure, causing “donut” shapes or fragmentation (Weatherly *et al.*, 2018).

In this study, we test the hypothesis that TCS inhibits mast cell function by depolarizing the plasma membrane. However, careful experimentation with two GEVI constructs, which function via disparate molecular machinery, indicate a wholly different mechanism of TCS action: cytoplasmic acidification. Furthermore, TCS replicates this mechanism of action and abrogation of function in another immune cell type, T cells.

## Methods

### Chemicals and Reagents

Triclosan (TCS; 99% purity; Sigma-Aldrich) was prepared in BT (Tyrodes buffer containing bovine serum albumin [BSA]) without use of organic solvent (Weatherly *et al.*, 2013) and diluted to deliver non-cytotoxic concentrations (Palmer *et al.*, 2012) checked by UV-Vis spectrophotometry (Weatherly *et al.*, 2013). Gramicidin (Sigma- Aldrich) was dissolved in 100% DMSO (Sigma-Aldrich) and diluted with BT.

### Cell Culture

RBL-2H3 mast cells were cultured as in (Hutchinson *et al.*, 2011).

Human Jurkat T cells, clone E6–1, were obtained from ATCC and maintained in suspension in phenol red-containing RPMI-1640 medium (ATCC) supplemented with 10% fetal bovine serum (Atlanta Biologics) and 100 U/ml penicillin-100 μg/ml streptomycin (Sigma-Aldrich). Cells were passaged once a week with thorough trituration technique to break up clumps, seeded at 35,000 cells/mL (for 6–7 days until harvest) to 125,000 cells/mL (for 3 days), and grown at 37°C and 5% $CO_2$. Supplement fresh media was added after 3 days in culture. These culturing conditions resulted in maximal cell density of 1–2 million cells/mL.

### Fluorescence Photoactivation Localization Microscopy (FPALM) Imaging and Processing

Three-dimensional FPALM mitochondrial imaging was performed as in (Parent and Hess, 2019). RBL cells were transfected with an expression vector for Dendra2-Tom20 (Weatherly

*et al.*, 2018) using an Amaxa transfection kit (Lonza), then plated in μ-Slide 8-well plates with polymer coverslip (ibidi) at 100,000 cells/well in 200 F06DL/well phenol red-free RBL media. The next day, cells were exposed to 20 μM TCS or BT for 1 hour and fixed with 4% paraformaldehyde (Sigma Aldrich) before imaging. Imaging was performed using a 558 nm laser (Crystalaser) for Dendra2-Tom20 excitation, and fluorescence was captured using an Olympus IX-71 microscope with 60X 1.45NA oil lens, 2X telescope, and an EMCCD camera (Andor iXon DU-897 #BV). Custom MATLAB analysis software was used to obtain localized data points (Hess *et al.*, 2006; Gudheti *et al.*, 2013; Curthoys *et al.*, 2019); details of microscopy are in Supplemental Methods.

### FPALM Mitochondrial Analysis

In MATLAB, raw data was localized first by fitting each Point Spread Function (PSF) to a two-dimensional (2D) Gaussian, which was then drift corrected. After drift correction, following the methods in (Huang *et al.*, 2008; Parent and Hess, 2019), the z-coordinate of each localized point was obtained from the measured calibration curve connecting the x- and y- widths of the PSF as a function of z- position. After obtaining the z-position for each localized point, the data set was processed through another custom MATLAB script for cluster identification, which compares the distances between each localization and all nearby localizations: localizations that lie within $d_{max}$ (75 nm) of each other are considered to be in the same cluster. Clusters with a minimum number of 50 localizations were analyzed further. The nearest-neighbor single linkage cluster analysis (SLCA) method (Sneath, 1957; Gudheti *et al.*, 2013) used here has been extended to three dimensions (Parent and Hess, 2019). Each cluster is then analyzed using the MATLAB convex hull and alpha shape functions, in order to quantify the local mean curvature for all localizations within an individual mitochondrion. Histograms and averages of the curvature, area, and volume of the convex and alpha hulls are then determined.

### Degranulation Assay

Degranulation assays were performed as in (Weatherly *et al.*, 2013), adapted for use with gramicidin in 0.003% DMSO vehicle. This fluorescence-based assay, performed in the 96-well format in a microplate reader, detects substrate cleavage by granule marker enzyme β-hexosaminidase in the supernatant from degranulating mast cells.

### $DiSC_3(5)$ Fluorescence Interference Assay

Triclosan effects on $DiSC_3(5)$ (TCI America) organic voltage sensitive dye fluorescence were assayed. The dye was dissolved in 100% DMSO. In a 96 well black bottom plate (Greiner), $DisC_35$ dye and TCS were mixed to achieve a final dye concentration of 1.02 μM in 0.01% final DMSO percentage, with various TCS concentrations (1–15 μM) in BT. The mixture was allowed to equilibrate for 10 min at 37°C. Fluorescence measurements were taken using a microplate reader (Synergy 2, Biotek) with 530 ± 20 nm excitation and 645 ± 15 nm emission.

### Plasma Membrane Potential and Cytosolic pH Assays in RBL-2H3 Mast Cells

In order to measure changes in plasma membrane potential, RBL cells were transfected with genetically-encoded voltage indicator (GEVI) protein construct ArcLight-A242 (a gift from Vincent Pieribone; Addgene plasmid # 36857; http://n2t.net/addgene:36857; RRID:Addgene_36857) (Jin *et al.*, 2012) or ASAP2 (pcDNA3.1/Puro-CAG-ASAP2s was a gift from Francois St-Pierre; Addgene plasmid # 101274; http://n2t.net/addgene:101274; RRID:Addgene_101274) (Chamberland *et al.*, 2017). To investigate TCS effects on cytosolic pH, RBL cells were transfected with plasma membrane-targeted Lyn-tailed mCherry-SuperEcliptic (SE) pHluorin protein construct (Lyn-tailed mCherry-SEpHlourin was a gift from Sergio Grinstein; Addgene plasmid # 32002; http://n2t.net/addgene:32002; RRID:Addgene_32002) (Koivusalo *et al.*, 2010). RBL cells were transiently transfected with ArcLight A242, ASAP2, or Lyn-tailed mCherry-SuperEcliptic (SE) pHluorin through electroporation using RBL-specific Amaxa Nucleofector transfection kit T (Lonza), then plated in 8-well plates (ibidi) at ~150,000 cells/well in 200 μL/well phenol red-free RBL media. Cells were grown for 16–24 hrs at 37°C/ 5% $CO_2$. Before imaging, cells were washed with BT and the media was replaced with 200 μL BT. After the initial, untreated, image was taken, cells were treated with 200 μL of either BT (for control) or various 2X concentrations of TCS or gramicidin, depending on the experiment. See “Confocal Microscopy” below for imaging details.

### Plasma Membrane Potential Assay in Jurkat T Cells

Ibidi 8-well plates were coated with 150 μL of human fibronectin (VWR) prepared at 166 μg/ml in phosphate buffered saline (PBS) (Lonza) (Wang *et al.*, 2019) overnight in the tissue culture incubator (37°C/5% $CO_2$); these wells were washed the next day with 200 μL PBS/ well before use. Jurkat cells were transiently transfected with ArcLight-A242 through electroporation using Jurkat-specific Amaxa Nucleofector transfection kit T (Lonza), then plated in the fibronectin pre-coated plates at ~1million cells/well in 300 μL phenol red-free Jurkat media. Cells were grown for 16–24 hours at 37°C/ 5% $CO_2$. Next day, cell media was removed carefully with a transfer pipette to avoid cell detachment and replaced with 200 μL control BT before imaging. After the initial, untreated, image was taken, cells were treated with 200 μL of either additional BT (for control) or various 2X concentrations of TCS. See “Confocal Microscopy” below for imaging details.

### Confocal Microcopy

For plasma membrane potential and cytosolic pH assays, an Olympus FV-1000 confocal microscope, with an Olympus IX-81 inverted microscope and a 30 milliwatt multi-argon laser, was used to collect images. ArcLight-A242 and ASAP2 plasmid-transfected cells were imaged using an oil immersion 100x objective with NA 1.4 and 488 nm excitation, 505–605 nm band pass emission filter. Lyn tailed mCherry-SEpHluorin transfected cells were imaged using oil immersion 60x objective with NA 1.4 and 488 nm excitation, 505–525 nm emission filter. All images were taken at 37°C using ibidi plate heating system.

## Manual Image Analysis

All image-analysis figures in this paper were generated with this manual method except for Figure 8 and Supplement Figure 3, which were analyzed with the automated image analysis procedure noted below. Confocal microscopy images of RBL and Jurkat cells transfected with ArcLight and ASAP2 were analyzed manually using Fiji ImageJ software (NIH). Well-transfected cells (i.e. visible expression of reporter and well-targeted to the plasma membrane) were identified and a Region of Interest (ROI) was drawn on the plasma membrane using the free-hand tool. The area of the ROI (in units of square pixels), integrated density (= sum of fluorescence intensity values of all pixels in the ROI), mean intensity (= integrated density divided by area of the ROI), and length of the ROI were subsequently measured at various specified time points before and after treatment.

Mean background fluorescence intensity (=integrated density of ROI divided by area of ROI) for a field of view, was obtained by either drawing a square shape ROI in the cytoplasmic region of transfected cells or by drawing an ROI around the plasma membrane of untransfected cells. Background mean fluorescence intensity obtained through either of these methods was subtracted from mean ArcLight fluorescence intensity of cells present in that field of view, and the resulting value at each time point was then normalized to (divided by) its own 0 min timepoint value of mean intensity. Both of these background subtraction methods resulted in similar ArcLight fluorescence changes due to 20 μM TCS: data for 7 cells selected randomly at the 15 min with 20 μM TCS, the cytosolic square shape method of background subtraction results in a calculated decrease of 36% ± 7% SEM in Arclight fluorescence while, for the same cells, the background subtraction method using a plasma membrane trace of untransfected cells results in a calculated decrease of 36% ± 8% SEM.

Photobleaching or drifting effect during imaging was calculated from BT-treated (control) cells by calculating a change in fluorescence values from 0 min. This change value was added/subtracted back to the treatment groups to account for these non-treatment effects and thus allowing measure of the true effect of a drug. Normalized values from multiple cells were averaged and used to generate line plots.

## Automated Image Analysis

In FIJI image J, individual images at different time points (0, 2, 5, 7, and 15 min) were converted to 8-bit stack. Background fluorescence was subtracted from the stack using pseudo flatfield correction. Next, by applying threshold, binary masks of the entire cell and only cytosol were created. Both of these masks were applied to transfected cells to obtain area of the ROI, integrated density, and mean intensity values. To find the area of the ROI, mean intensity and integrated density of plasma membrane, values of cytosol were subtracted from the area of the ROI and integrated density of whole cell. The calculated integrated density was divided by the calculated area of ROI. This will give mean fluorescence intensity of the plasma membrane. Mean intensity at different time points of an individual cell was normalized to (divided by) its own 0 min time point value of mean intensity. Fluorescence was adjusted for drifting or photobleaching as described in “Manual Image Analysis” Methods above. This automated method was utilized to generate Figure 8 and Supplement Figure 3.

### Analysis of Triclosan Effects on ArcLight-A242 Fluorescence Intensity as a Function of Initial ArcLight-A242 Expression Level

Initial (0 min) mean plasma membrane fluorescence intensity of ArcLight for each individual cell was noted. Next, for each individual cell, the percentage drop in ArcLight fluorescence mean intensity incurred by 15 min exposure to 20 μM triclosan (or to control BT) was then plotted as a function of that cell's initial mean intensity of ArcLight (its expression level of the construct). Linear regression analysis was performed, and the slope of the best-fit line and $R^2$ value was determined for each plot.

### Apparent Plasma Membrane Potential Percentage Decrease Calculation

Apparent PMP percentage decrease was calculated for the treatments, cell types, and GEVIs utilized in this study. Each normalized and photobleaching-/drift-corrected GEVI fluorescence value was subtracted from 1 to determine change in fluorescence due to treatment. This result was subsequently multiplied by its respective reporter's PMP to fluorescence change ratio to calculate mV change as reported by each construct. For ArcLight-A242, this ratio is 100 mV for every 35% decrease in fluorescence (100 mV/0.35) (Jin *et al.*, 2012). For ASAP2, this ratio is 100 mV for every 39% decrease in fluorescence (100 mV/0.39) (Chamberland *et al.*, 2017). This change, in units of mV, was then divided by the resting PMP of the corresponding cell type, RBL mast cell (−82.5 mV is the average value from two patch-clamp studies (Lindau and Fernandez, 1986; Wischmeyer *et al.*, 1995)) or T cell (−60 mV)(Sarkadi *et al.*, 1990) to determine the (unitless) change in total resting cell PMP. Finally, this result was subsequently subtracted from 1 and multiplied by 100 to obtain the apparent PMP percentage.

### TCS Cytotoxicity on Jurkat Cells

Trypan blue exclusion and lactate dehydrogenase (LDH) cytotoxicity assays were used to assess TCS cytotoxicity on Jurkat cells. In the trypan blue exclusion assay, 1 million cells were plated into each of 3 wells of a 24-well, flat-bottom cell culture plate (Costar) for TCS (Sigma) treatment and 3 wells for the control. Immediately after plating, BT and 2X TCS doses were added to respective wells. Next, cells were incubated for 30 minutes at 37°C/5% $CO_2$. After the incubation, a small sample was taken from each well and mixed 1:1 with trypan blue dye (0.4%, Lonza) evenly. Cells were counted using a hemocytometer for viability and TCS-treated cells were normalized to the control. LDH cytotoxicity methods were those of Hutchinson *et al.*, 2011 using a cytotoxicity detection kit (Roche). However, the lysis solution was added to the "high control" in the final 15 minutes of the 1-hour TCS exposure instead of an additional 15 minutes after the 1-hour TCS exposure (Palmer *et al.*, 2012).

### Cytosolic $Ca^{2+}$ assay

Prior to performing $Ca^{2+}$ assays, widefield fluorescence microscopy was used to assess transfection efficiency of GCaMP6 $Ca^{2+}$ reporter construct in Jurkat T cells, and $Ca^{2+}$ assays were performed only on samples of highly-transfected cells. First, 8-well ibidi plates were coated with 150 μL/well fibronectin (166 μg/ml) prepared in PBS and incubated overnight in tissue culture incubator. The next day, Jurkat T cells were transfected with pGP-CMV-

GCaMP6f (a gift from Douglas Kim & GENIE Project; Addgene # 40755; http://n2t.net/addgene:40755; RRID: Addgene_40755) (Chen *et al.*, 2013) using Jurkat specific Amaxa Nucleofector transfection kit T (Lonza). The electroporated cells were plated in phenol red-free Jurkat cell media at ~1 million cells/well with phenol red-free media in the fibronectin pre-coated 8-well ibidi plates. Cells were grown for 16–24 hours at 37°C/ 5% $CO_2$. The next day, cell media was removed carefully with a transfer pipette to avoid cell detachment and replaced with 200 μL BT, and images were taken with a wide-field IX83 (Olympus, Waltham MA) microscope with a Prime 95B CMOS Camera (Photometrics) and HLD117 stage (Prior Scientific) controlled by a Proscan III. Fluorescence excitation was provided by an Xcite 120 LEDBoost (Excelitas). Images were taken at 60x (Olympus-APON-60X-TIRF objective) using standard excitation and emission filters for GFP (Semrock). The microscope is controlled by CellSens software v1.18 (Olympus).

For assessment of Jurkat T cell cytosolic $Ca^{2+}$ levels following anti-T cell receptor (anti-TCR) stimulation, a plate reader assay was performed similarly to that in (Weatherly *et al.*, 2018), with the following modifications. First, a 96-well, black-walled, clear-bottom plate (Grenier) was coated overnight with 50 μL/well fibronectin (166 μg/ml) prepared in PBS (Lonza). The next day, cells were transfected with the GCaMP6 construct as noted above and plated in 200 μL/well phenol red-free media in the fibronectin pre-coated 96-well plate at 330,000 cells/well. Cells were cultured overnight at 37°C and in 5% $CO_2$. Next day, media was carefully aspirated from wells with a micropipette to avoid cell detachment, and cells were exposed to 100 μL/well 0.2 μg/ml (Holowka *et al.*, 2018) Anti-TCR OKT3 monoclonal antibody (Thermo Fisher Scientific) in combination with control BT or TCS treatments for 1 hour. Fluorescence was measured with 485 ± 10 nm excitation and 528 ± 10 nm emission during this 1 hour. Area under the curve was determined as per methods in Weatherly *et al.*, 2018.

## Statistical Analyses

All analyses were performed in Graphpad Prism. In most figures, raw values for treatment groups were normalized to its appropriate untreated control. Biological replicates from at least three independent experiments were averaged, and standard error of the mean (SEM) was calculated across those independent experiments. Raw (non-normalized) values were analyzed for mitochondria swelling and LDH release experiments (Figures 1, 6D). One-way ANOVA followed by Tukey's *post-hoc* test ($\alpha$=0.05) was used to determine the significance level of most experiments (Figures 2, 3B, 5, 6, 7B, 8, Supplement Figures 2–6). The significance level of the FPALM mitochondrial volume and surface area were assessed using an unpaired one-tailed t-test (Figure 1). The significance level of the cytosolic $Ca^{2+}$ level area under the curve (AUC) of Jurkat cells was assessed via paired t-test (Figure 9B). Significance is represented by ***$p$<0.001, **$p$<0.01, and *$p$<0.05.

## Results

### Triclosan increases mitochondrial volume and surface area in RBL-2H3 mast cells: Indicators of inhibited mitochondrial membrane potential

Previously, an organic dye fluorescence method (without imaging) revealed that TCS inhibits MMP (Weatherly *et al.*, 2018). To test this finding at the nanoscale, three-dimensional super-resolution FPALM imaging (Huang *et al.*, 2008; Parent and Hess, 2019) was employed to assess TCS effects on 3D mitochondrial morphology, changes in which are linked to inhibition of MMP (Guillery *et al.*, 2008; Giedt *et al.*, 2012; Weatherly *et al.*, 2018). RBL cells were transiently transfected with Dendra2-TOM20 (Weatherly *et al.*, 2018), a construct used to label the outer membrane of mitochondria. The next day, cells were exposed with TCS or BT control for 1 hour, then fixed using paraformaldehyde. While the TCS effects on mitochondrial volume and surface area were not dramatic visually (a no-TCS control figure is shown in Supplement Figure 1), they were statistically significant when analyzed quantitatively. Triclosan statistically significantly increases the mean volume, as calculated by the convex hull method, by 17% compared to control (Figure 1A). Also, triclosan increases the mean mitochondrial surface area, as calculated by the alpha shape method, by 19% (Figure 1B). Thus, TCS modulates the surface area and volume of individual mitochondria, as assessed with 3D FPALM super-resolution microscopy.

### Plasma membrane potential depolarizer gramicidin potently inhibits the degranulation of RBL-2H3 mast cells

To determine the effects of the canonical plasma membrane depolarizer, gramicidin, on RBL mast cell degranulation, an adapted fluorescence-based β-hexosaminidase release assay (Weatherly *et al.*, 2013) was employed. A multivalent DNP (dinitrophenol)-BSA Ag was used to laterally crosslink IgE-bound FcεRI receptors, thus initiating an allergic/pro-inflammatory signal transduction that ends with the release of granules containing bioactive substances including β-hexosaminidase, which is monitored fluorometrically. Gramicidin depolarizes cells by forming an ion channel at the plasma membrane, allowing for free passage monovalent ions such as $H^+$, $NH_4^+$, $K^+$, $Na^+$, and $Li^+$ down their concentration and electrochemical gradients, and, thus, depolarizing the plasma membrane (Myers and Haydon, 1972; Mohr and Fewtrell, 1987b).

Figure 2A presents the results for IgE-sensitized RBL cells incubated for 1 h in Tyrodes—BSA (BT) buffer containing a 0.0004 μg/ml Ag dose, with gramicidin or DMSO vehicle. All tested gramicidin doses, as low as 0.1 μM, inhibit degranulation, reducing the response down to the same level as the spontaneous group (unstimulated with Ag). These data indicate a potent, plasma membrane depolarization-mediated inhibition of degranulation. A similar, but slightly less potent, gramicidin-induced depression of degranulation can be seen in the group treated with the higher Ag dose, 0.001 μg/ml Ag (Figure 2B). In this case, statistically significant inhibition of degranulation does not begin until 0.5 μM gramicidin and appears to proceed in a dose-responsive fashion. Such data coincide with the previously reported observation that pharmacologically induced inhibition of degranulation occurs at lower toxicant doses when cells are stimulated at a low level (0.0004 μg/ml Ag) than when stimulated at a high level (0.001 μg/ml Ag) (Palmer *et al.*, 2012).

A dose comparison study for gramicidin and TCS was performed as part of testing the hypothesis that TCS inhibits degranulation via PMP inhibition, by repeating the above experiments with TCS in place of gramicidin at equivalent antigen and DMSO concentrations. While DMSO is not needed/used here to dissolve the TCS, it was included to match the conditions of the gramicidin experiments. Statistically significant, dose-responsive inhibition of mast cell degranulation by TCS is reported in Figures 2C and 2D, beginning at 10 μM (Figure 2C). This observation recapitulates previously observed TCS-mediated inhibition of degranulation (Palmer *et al.*, 2012), but the presence of DMSO reduces its potency: 10 μM TCS inhibits 0.0004 μg/ml Ag-stimulated degranulation by about one-half in the absence of DMSO (Weatherly *et al.*, 2013) and only by about one-third in the presence of 0.003% DMSO (Figure 2C). Also, the TCS inhibitory effect lessens in the presence of higher Ag dose (0.001 μg/ml Ag; Figure 2D), as noted with gramicidin Figure 2B. Overall, depolarizer-mediated inhibition of degranulation (Figure 2A and 2B) proceeds similarly as that of TCS, though gramicidin is more potent than TCS, especially in the presence of DMSO. The result strengthens the connection between PMP inhibition and degranulation inhibition.

### Gramicidin and triclosan depress ArcLight-A242 fluorescence in RBL-2H3 mast cells.

Gramicidin, a known depolarizer of PMP, strongly inhibits degranulation (Figs. 2A and 2B), and TCS also reduces degranulation (Palmer *et al.*, 2012). Also, TCS depolarizes the MMP (Weatherly *et al.*, 2018) (Figure 1). Thus, we hypothesized that TCS also inhibits the PMP, as its underlying mechanism of degranulation inhibition. To do so, an organic voltage-sensitive fluorescent dye, $DiSC_3(5)$ was employed. However, when TCS (micromolar levels) and $DiSC_3(5)$ (1 μM) (Te Winkel *et al.*, 2016) are mixed together in the absence of cells, TCS chemically quenches the fluorescence of $DiSC_3(5)$ in a dose-response manner (Supplement Figure 2); thus, $DiSC_3(5)$ cannot be used to accurately measure TCS effects on PMP. Triclosan quenching of unprotected fluorophores (such as those found in various voltage-sensitive, fluorescent organic dyes) has previously been observed (Weatherly, 2017; Weatherly *et al.*, 2018). Thus, to measure TCS effects on PMP, genetically encoded voltage indicators (GEVIs), which contain β-barrel protein structures which may protect their fluorophores from chemical quenching or aggregation effects (Chalfie and Kain, 2005), were used. Triclosan does not interfere with the fluorescence of the fluorescent protein within the reporter construct GCaMP (Weatherly *et al.*, 2018).

To measure PMP of cells using a GEVI, RBL cells were transiently transfected with ArcLight-A242 (ArcLight) (Jin *et al.*, 2012) (Figure 3A). The next day, confocal images were collected for each cell at different time points, up to 15 minutes, before (Figure 3A) and after (Figure 3B) addition of control (BT), TCS, or gramicidin. Fluorescence obtained was quantified using FIJI image J (Manual Image Analysis Methods) and normalized to the 0 min time point for each condition. Gramicidin, a known PMP depolarizer, statistically significantly reduces ArcLight fluorescence within 2 min of exposure and by 23% (± 2% SEM) at the end of 7 minutes. TCS, at 20 μM, statistically significantly lowers ArcLight fluorescence within 5 min of exposure and by 25% (± 3% SEM) at the end of 15 min. This result was further confirmed by an automated image analysis method (Supplement Figure 3). The 10 μM TCS data suggest an inhibition of ArcLight fluorescence by 15 min but were not

statistically significant. The decrease in ArcLight fluorescence suggests that both gramicidin and TCS inhibit mast cell PMP.

Since gramicidin treatment contained DMSO vehicle (0.003%), it was important to determine whether gramicidin's effects on ArcLight fluorescence are modulated by the presence of DMSO. Thus, a control experiment was performed by repeating the gramicidin-ArcLight experiments in the presence of varying DMSO concentrations. Gramicidin's ability to inhibit ArcLight fluorescence is unaffected by increasing DMSO concentrations, ranging from 0.003% to 0.01% (Supplement Figures 4 and 5).

After experiments with transiently-transfected cells were successfully conducted, ArcLight stably-transfected cell lines were created, with the goal of enabling high-throughput testing of numerous concentrations of triclosan and other toxicants, as well as additional time points. However, unfortunately, clones of RBL cells stably transfected with ArcLight display construct aggregation and poor plasma membrane localization (Supplement Figure 6).

To check whether plasmid expression level affects the change in GEVI fluorescence in response to triclosan, the initial, 0 min (pre-triclosan-exposure), background-subtracted mean fluorescence intensity of each individual cell from Figure 3's data was analyzed. The percentage drop in ArcLight fluorescence by 15 minutes time of exposure (control buffer-treated in 4A, TCS-treated in 4B), for each individual cell, was plotted as a function of that particular cell's initial mean intensity of ArcLight. There is no correlation between plasmid expression level and the magnitude of TCS inhibition of ArcLight fluorescence (Figure 4B), as analyzed by linear regression. Thus, TCS effects on GEVI fluorescence are unaffected by the "brightness" (GEVI expression level) of the cell.

Plasma membrane depolarization causes ArcLight fluorescence intensity to decrease, in a linearly proportional fashion (Jin *et al.*, 2012). PMP percentage decline can be calculated from the measured change in ArcLight fluorescence, as outlined in Methods. This apparent mast cell PMP, as a percentage of initial, 0 min, pre-triclosan-exposure value, is plotted as a function of time following TCS or gramicidin exposure (Figure 5). Within 7 min of exposure to 1 μM gramicidin, RBL mast cell PMP appears to decrease by 79% (± 7% SEM) of initial resting PMP. Similarly, within 15 min of exposure to 20 μM TCS, RBL cell PMP appears to decrease by 90% (± 11% SEM). There appears to be a modest, but not statistically significant, decline in PMP within 15 min exposure to 10 μM TCS.

Triclosan inhibits ArcLight fluorescence, and, thus, apparently inhibits RBL cell PMP. Thus, the next experiments tested whether these results are extendable to another immune cell type which is also dependent on PMP and SOCE for its function, T-cells.

### Non-cytotoxic doses of triclosan depress ArcLight-A242 fluorescence in Jurkat T cells.

To measure triclosan effects on PMP of T cells, human Jurkat T cells were transiently transfected with ArcLight. The next day, confocal images were collected for each cell at different time points, up to 15 minutes, before and after addition of control (BT) or TCS (Figure 6A). Fluorescence obtained was quantified using FIJI image J (Manual Image Analysis Methods) and normalized to the 0 min time point for each condition. TCS, at 20

μM, lowers ArcLight fluorescence within 2 min of exposure and by 31% (± 3% SEM) at the end of 15 min (Figure 6A). The decrease in ArcLight fluorescence suggests that TCS inhibits T cell PMP.

This apparent T cell PMP was calculated (see Methods) as a percentage of initial, 0 min, pre-triclosan-exposure value and is plotted as a function of time following TCS exposure (Figure 6B). Within 15 min of exposure to 20 μM TCS, T cell PMP appears to decrease to −150% (± 15% SEM) of initial resting PMP, apparently a more-than-complete dampening of T cell PMP.

In order to determine if the results obtained above were truly functional changes or due to cytotoxicity from TCS, the effect of micromolar doses of TCS (0 μM, 10 μM, and 20 μM) on Jurkat T cell viability were assessed using a trypan blue exclusion assay. Results indicate that TCS does not cause a decrease in cell viability within a 30 min exposure (Figure 6C). In order to confirm these cytotoxicity results, a more sensitive microplate reader-based assay, LDH assay was also performed. LDH release was measured in response to varying doses of TCS for 1 hour. There is no significant release of LDH from TCS-treated cells as compared to control; the “high control” sample is a positive control detecting LDH release from lysed cells (Figure 6D). These data from cytotoxicity experiments indicate that TCS dosage timing and concentration used in this study do not cause Jurkat T cell cytotoxicity.

## Triclosan does not depress the fluorescence of the genetically encoded voltage indicator ASAP2 in RBL-2H3 mast cells.

To check the results obtained using ArcLight, an alternative GEVI, called ASAP2, which utilizes a different voltage-sensing mechanism from that of ArcLight (Jin *et al.*, 2012; Chamberland *et al.*, 2017) was used. RBL mast cells were transiently transfected with ASAP2 (Figure 7A). The next day, confocal images were collected for each cell at different time points, up to 15 minutes, before (Figure 7A) and after (Figure 7B) addition of control (BT) or TCS. Fluorescence obtained was quantified using FIJI image J (Manual Image Analysis Methods) and normalized to 0 min time point for each condition. Triclosan (20 μM, up to 15 min) does not alter fluorescence of ASAP2 when compared to the 0 μM TCS control (Figure 7B). In stark contrast to the clear triclosan dampening of fluorescence observed with the ArcLight reporter (Figure 3), these ASAP2 results (Figure 7B) indicate that TCS does not change the PMP of RBL mast cells.

However, TCS inhibits the fluorescence of ArcLight, which contains a pH-sensitive super ecliptic pHlourin on the cytoplasmic side of the plasma membrane. Thus, the next investigation centered on whether TCS-induced depression of ArcLight fluorescence is due to a change in cytosolic pH instead of a change in PMP.

## Triclosan depresses fluorescence of a plasma membrane-targeted pHlourin in RBL mast cells, indicating triclosan reduction of cytosolic pH.

To identify whether TCS affects cytosolic pH, plasma membrane-targeted fluorescence reporter called Lyn-tailed mCherry-SEpHlourin (Koivusalo *et al.*, 2010), which measures sub-plasma membrane cytosolic pH of a cell, was employed. The transfection and imaging procedures used for the GEVI experiments were repeated, along with an automated image

analysis technique (described in Methods). Triclosan, at 20 μM, decreases mCherry-SEpHlourin fluorescence intensity within 5 min of exposure and by 43% (± 2% SEM) at the end of 15 min (Figure 8). This result is similar to the magnitude of triclosan's effect on ArcLight fluorescence (Figure 3), suggestive of a pH change in response to TCS rather than a PMP change.

### TCS inhibits cytosolic $Ca^{2+}$ response to Anti-T Cell Receptor stimulation in Jurkat T cells

TCS affects $Ca^{2+}$ dynamics and inhibits SOCE in mast cells (Weatherly *et al.*, 2018). Due to the similar triclosan depression of ArcLight fluorescence in Jurkat T cells (Figure 6A) as in RBL mast cells (Figure 3B), we hypothesized that a similar calcium effect also occurs in Jurkat T cells. To test this hypothesis, Jurkat T cells were transfected with $Ca^{2+}$ reporter construct GCaMP6 (Chen *et al.*, 2013). The next day, cells were stimulated with 0.2 μg/ml Anti-T Cell Receptor (TCR) OKT3 ± TCS (Holowka *et al.*, 2018), and cytosolic $Ca^{2+}$ was measured throughout the duration of 1 hour. Cells were transfected at a highly efficient rate (Supplement Figure 7). Following anti-TCR stimulation, an initial rise in $Ca^{2+}$ is seen within the first few minutes, followed by a plateau $Ca^{2+}$ level above unstimulated basal level (compare "0 μM TCS + Ab" to "Unstimulated" curves in Figure 9A), as expected (Holowka *et al.*, 2018). TCS, at 20 μM, inhibits $Ca^{2+}$ levels in comparison to the control in anti-TCR activated cells, in particular by flattening the plateau region (Figure 9A). Triclosan minimally affects the initial $Ca^{2+}$ rise but heavily dampens calcium in the plateau region, similar to its effects in RBL mast cells (Weatherly *et al.*, 2018). AUC analysis reveals an average decrease of 70% (± 17%) integrated $Ca^{2+}$ levels in anti-TCR activated cells with TCS treatment compared to that of activated control (Figure 9B).These data indicate that TCS inhibits cytosolic $Ca^{2+}$ signaling in T cells.

## Discussion

Triclosan disrupts mast cell function, rapidly (within tens of minutes) and at non-cytotoxic concentrations relevant to consumer product exposure (Palmer *et al.*, 2012; Shim *et al.*, 2019), but the underlying biochemical mechanism was unknown. In this study, we deduced the mode of action of TCS in mast cells and replicated these TCS effects in another immune cell type, T cells.

The process of deciphering the mechanism began with two observations: TCS is a mitochondrial uncoupler (Weatherly *et al.*, 2016; Weatherly *et al.*, 2018) and also a disruptor of the central signal for mast cell degranulation—cytosolic $Ca^{2+}$ rise (Weatherly *et al.*, 2018). As an uncoupler, TCS depresses the MMP, which results in mitochondrial fragmentation, observed in live cells with super-resolution microscopy (Weatherly *et al.*, 2018). Mitochondrial toxicity and deformation are important markers of TCS toxicity in numerous cell types and species (Shim *et al.*, 2016; Weatherly *et al.*, 2018; Weatherly *et al.*, 2020). Disruption of mitochondrial shape plays a role in diseases such as cognitive decline (Hara *et al.*, 2014), Parkinson's disease (Cui *et al.*, 2010; Bhandari *et al.*, 2014), insulin resistance (Jheng *et al.*, 2012), immune dysfunction (Weatherly *et al.*, 2020), inflammation (Compan *et al.*, 2012), and disrupted embryonic development (Chen *et al.*, 2003). In this study (Figure 1), we have augmented these findings by utilizing 3D super-resolution FPALM

to reveal TCS enhancement of mitochondrial surface area and volume, indications of mitochondrial swelling and MMP disruption (Guillery *et al.*, 2008; Giedt *et al.*, 2012). This increase in surface area and volume has also been observed in neuronal mitochondria due to exposure to carbonyl cyanide-4 (trifluoromethoxy)phenylhydrazone (FCCP), a known proton ionophore and MMP depolarizer (Safiulina *et al.*, 2006). The connections between mitochondrial deformation and disrupted MMP are extended to PMP depolarization, inhibited store-operated calcium entry (SOCE), and, subsequently, dampened mast cell degranulation via studies with a similar proton ionophore mitochondrial uncoupler, carbonyl cyanide *m*-chlorophenylhydrazone (CCCP), which also inhibits MMP, PMP, SOCE, and mast cell degranulation (Mohr and Fewtrell, 1987b). Triclosan's enhancement of mitochondrial surface area and volume led to a PMP collapse hypothesis as the mode of action of immune cell dysfunction.

Thus, we hypothesized that TCS inhibits not just MMP but also PMP. Direct evidence for this hypothesis was provided by reports that TCS induces an electrical current (evidence of its proton ionophore nature) across artificial membranes (Popova *et al.*, 2018) and depolarizes neuronal PMP (Arias-Cavieres *et al.*, 2018; Popova *et al.*, 2018) at micromolar doses within tens of minutes. As calculated in the Introduction, a complete depolarization of PMP in mast cells would lead to a ~45% reduction in the driving force for cytosolic $Ca^{2+}$ influx into the cell through activated CRAC channels; indeed, Weatherly et al., 2018 reported ~45% decrease in cytosolic calcium levels after TCS exposure in RBL mast cells. This study also reports (Figure 9) a robust decrease in cytosolic calcium levels after TCS exposure in Jurkat T cells. In turn, the decrease in cytosolic $Ca^{2+}$ inhibits degranulation (Holowka *et al.*, 2012). Additionally, the known PMP depolarizer gramicidin inhibits mast cell degranulation in parallel conditions to TCS mast cell disruption (Figure 2), lending further support for the PMP collapse hypothesis for the TCS mode of action.

To measure TCS effects on PMP, two genetically encoded voltage indicator (GEVI) reporter constructs, ArcLight-A242 (ArcLight) (Jin *et al.*, 2012) and ASAP2 (Chamberland *et al.*, 2017), were utilized. ArcLight senses changes in PMP due to its two specialized subunits: a transmembrane voltage-sensing domain which, upon changes in PMP, undergoes conformational changes that cause conformational changes in the attached green fluorescent protein (GFP)-derived, super ecliptic pHlourin fluorescent domain which is localized intracellularly, in the cytosol. ASAP2 also contains a transmembrane voltage-sensing domain but, in contrast to ArcLight, ASAP2 contains an extracellularly-located, circularly-permuted (non-pHlourin-based) fluorescent GFP (cpGFP) domain. For both of these GEVIs, their fluorescence intensity decreases upon PMP depolarization. These experiments yielded drastically different results: Triclosan inhibits ArcLight fluorescence in RBL mast cells (Figure 3) and in Jurkat T cells (Figure 6), suggesting TCS-induced collapse of PMP in these cell types (Figures 5 and 6). Note that the effect was not statistically significant with 10 μM TCS but did suggest a modest inhibition at that dose/timeframe. In contrast, TCS had no effect on ASAP2 fluorescence (Figure 7). While both ArcLight and ASAP2 are plasma membrane voltage-sensitive, there is a crucial difference in their structures: the location and pH sensitivity of their fluorescent protein domains. ArcLight's fluorescent domain is a pHlourin, which is strongly pH-sensitive in the physiological pH range (Jin *et al.*, 2012) (Supplement Figure 2B from this article shows that a pH reduction from 7.5 to 6.5 would

drastically reduce this pHlourin's intensity, by ~50% or more). It is located in the cytosol, so it reports changes in cytosolic pH, with acidification leading to fluorescence intensity decline. ASAP2 cannot report cytosolic pH changes because its fluorescent domain is located outside the cell, unless those changes affect the PMP (personal communication, Dr. Francois St-Pierre). Interpretation of the ASAP2 data is somewhat confounded by the fact that its cpGFP fluorescent domain is also somewhat pH sensitive (Miyawaki and Niino, 2015; Kostyuk *et al.*, 2019). While TCS mitochondrial toxicity could lead to extracellular acidification which could affect ASAP2 fluorescence, TCS-induced extracellular acidification likely occurs on a longer timescale (Ajao *et al.*, 2015) than the 15 min exposure assessed in the current study. Also, if TCS were acidifying the extracellular space around the RBL mast cells and Jurkat T cells within the experimental exposure time (15 min), overcoming the buffering of the BT solution, a decrease in ASAP2 fluorescence would have occurred (Stepanenko *et al.*, 2008). Together, these data suggest that TCS does not affect mast cell or T cell PMP but, instead TCS lowers cytosolic pH.

Indeed, TCS acidifies the cytosol, as measured with lyn-tailed mCherry-SEpHluorin, a pH-sensitive, PMP-insensitive reporter construct (Figure 8). ArcLight and lyn-tailed mCherry-SEpHluorin share the same pH-sensitive fluorophore, the super ecliptic pHlourin (Koivusalo *et al.*, 2010; Jin *et al.*, 2012). A decrease in lyn-tailed mCherry-SEpHluorin's fluorescence is equivalent to a cytosolic pH decrease (Koivusalo *et al.*, 2010). This intracellular pH effect may either be localized, or be most drastic, near the plasma membrane itself as both of these pH-sensitive reporters are plasma membrane-localized (Koivusalo *et al.*, 2010; Jin *et al.*, 2012). As noted in Methods, a 35% decrease in the fluorescence intensity of ArcLight corresponds with a 100 mV PMP decrease (Jin *et al.*, 2012); thus, a 29% decrease in fluorescence intensity would correspond with a complete depolarization of the RBL cell PMP (~82.5 mV) (Lindau and Fernandez, 1986; Wischmeyer *et al.*, 1995). Thus, if the ArcLight response were measuring PMP changes in response to TCS, the maximum response of any cell should have been ~29%. On the contrary, nearly half of cells responded to TCS exposure with a greater-than-29% drop in ArcLight fluorescence (Figure 4). Some of this variation is likely due to cell-to-cell variation in signaling, even in this clonal cell line (Millard *et al.*, 1988).

However, because ArcLight's fluorescence can also communicate changes in pH and can be depressed nearly 100% within a 1 pH unit acidification starting at normal physiological pH (Jin *et al.*, 2012), the cell-to-cell variation of TCS response in Figure 4 provides further evidence for TCS acidification of the cytosol.

Taking into account the pH sensitivity of its fluorophore (Jin *et al.*, 2012), the ArcLight data (Figure 3) can be re-interpreted as a 20 μM TCS-induced pH decrease of −0.23 pH units (Table 1). The pH sensitivity of the fluorescence intensity of ArcLight's super ecliptic A227D pHlourin (plotted in the Supplement of (Jin *et al.*, 2012)) is approximately linear between pH 6.5 to 7.5. This relationship can be approximated using the following: $F = 0.6pH - 3.8$ where F is the fraction of maximal fluorescence, and the equation is valid over a range of ± 0.5 pH units. Thus, at a pH of 7.2, F = 0.52, meaning that ArcLight will exhibit 52% of its maximal fluorescence intensity at the starting, physiological pH. The 26% ± 3% (SEM) decline in ArcLight fluorescence due to 15 min of 20 μM TCS exposure (Figure 3)

translates to a 26% reduction in this 0.52 value, bringing the final, normalized, ArcLight fluorescence intensity to 0.38 ± 0.02; solving for the corresponding pH value returns a final pH value of 6.97 ± 0.02 following this TCS exposure. This yields the −0.23 pH unit decrease estimate from the ArcLight data (Table 1). Additionally, the same data interpretation can be employed with lyn-tailed mCherry-SEpHluorin, resulting in a pH decrease to 6.83 ± 0.02, yielding the −0.37 pH unit decrease estimate (Table 1). These pHlourin-measured decreases in pH are similar in magnitude, providing corroborating evidence that TCS acidifies the cytosol.

These measured pH changes were confirmed with theoretical calculations of TCS acid-base chemistry. Taking into account the 400 μL volume of 20 μM TCS in each ibidi well containing ~400,000 cells on each experimental day (see Methods), along with an estimated 10% absorption rate (Moss *et al.*, 2000; Weatherly and Gosse, 2017), each cell received ~5.3 × $10^{-15}$ moles, or 3.2 × $10^{9}$ molecules of TCS. Considering its pKa of 7.9 (PubChem), a resting cell cytosolic pH of 7.2 (Johnson *et al.*, 1980; Lodish *et al.*, 2000; Beck *et al.*, 2014), and the Henderson-Hasselbalch equation, 16.6% of TCS is deprotonated when it encounters the pH 7.2 resting cytosol. This 16.6% value equates to 5.3 × $10^{8}$ deprotonated TCS molecules per cell, and hence, 5.3 × $10^{8}$ excess $H^{+}$ delivered to each cell as this monoprotic weak acid dissociates. While this excess proton dose, from TCS, far exceeds the proton concentration of the cell, it rapidly encounters the cellular buffering system. Carbonate ($CO^{2}/HCO_{3}^{-}$, pKa 6.1) buffering (Nelson and Cox, 2017) accounts for approximately two-thirds of a cell's total buffering power (Boron, 2004), and average mammalian cells contain 12 mM of $HCO_{3}^{-}$ (Lodish *et al.*, 2000), the conjugate base of this buffering system ($A^{-}$); these values and the Henderson-Hasselbalch equation can be used to calculate the concentration of the weak acid (HA) in the untreated cell: 0.953 mM. The average mammalian cell has a volume of 1766 $\mu m^{3}$ (Barrandon and Green, 1985), and the cytosol itself accounts for 70% cellular volume (Luby-Phelps, 2000). Thus, the volume of the cytosol is 1236 $\mu m^{3}$ or 1.236 ×$10^{-12}$ L. Multiplying this volume by the HA and $A^{-}$ concentrations noted above and by Avogadro's number yields the number of HA and $A^{-}$ molecules found within the cytosol of an untreated cell: 7.1 × $10^{8}$ HA molecules and 8.9 × $10^{9}$ $A^{-}$ molecules. The 5.3 × $10^{8}$ excess $H^{+}$ delivered to the cell by TCS exposure interact 1:1 with these $A^{-}$ molecules, thereby producing 5.3 × $10^{8}$ new HA molecules added to the original pool of HA molecules and subtracted from the original pool of $A^{-}$ molecules: resulting in 1.24 × $10^{9}$ molecules of HA and 8.4 × $10^{9}$ $A^{-}$ molecules. Plugging these values into the Henderson-Hasselbalch equation leads to a cytosolic pH of TCS-treated cells of 6.9: a −0.3 pH depression caused by TCS exposure (Table 1). In fact, the average of the pH depressions captured in the ArcLight and lyn-tailed mCherry-SEpHluorin measurements is −0.3, in agreement with this calculated value.

Acidification of the cytosol has been shown to decrease $Ca^{2+}$ release-activated $Ca^{2+}$ current ($I_{CRAC}$), the final step in SOCE, in several cell types including RBL and Jurkat T cells expressing stromal interaction molecule 1 (STIM1) and ORAI1 (Beck *et al.*, 2014). In the Beck study, the cytosol of each assayed cell was acidified via direct introduction of NaOH or HCl via pipette. In the current study, the cytosol was acidified by exposure to TCS (a weak acid, pKa 7.9) via the extracellular buffer (Table 1), rather than by direct injection of strong acid or base (Beck *et al.*, 2014). A stepwise effect, reduction of $I_{CRAC}$, occurred upon

decreasing the pH from 7 to 6 (Beck *et al.,* 2014). Similarly, TCS reduces $Ca^{2+}$ flux into the cytosol of RBL and Jurkat cells (Weatherly *et al.*, 2018) (Figure 9). Triclosan-mediated acidification of the cytosol may thus explain the previously observed inhibition of $Ca^{2+}$ dynamics (Weatherly *et al.*, 2018) and, thus, of degranulation (Holowka *et al.*, 2012).

Another proton ionophore mitochondrial uncoupler, CCCP, also inhibits $Ca^{2+}$ influx into RBL mast cells (Mohr and Fewtrell, 1987b). While this effect is partly caused by CCCP's depolarization of PMP (Mohr and Fewtrell, 1987b), it can also be reversed by increasing the pH (i.e. alkalization) of the surroundings (Mohr and Fewtrell, 1987b) and, hence, of the cytosol because $H^+$ becomes plasma membrane-permeant when CCCP is incorporated into the membrane (McLaughlin and Dilger, 1980). These findings suggest that CCCP inhibition of SOCE is partly caused by its pH modulation. Additionally, experiments on isolated neurons have shown that another proton ionophore mitochondrial uncoupler, FCCP, also acidifies the cytosol (Tretter *et al.*, 1998). Therefore, TCS is acting as expected, from its proton ionophore mitotoxicant nature, in acidifying the immune cell cytosol and, then, inhibiting SOCE.

While under some conditions acidification of the cytoplasm can inhibit SOCE by blocking the binding of $IP_3$ to its receptor on the ER (Tsukioka *et al.*, 1994), release of $Ca^{2+}$ from the ER is actually enhanced in TCS-treated mast cells (Weatherly *et al.*, 2018). Following anti-TCR activation of SOCE in T cells, the initial rise of $Ca^{2+}$ release from the ER is largely unaffected by TCS whereas the plateau region representing SOCE via CRAC channels is heavily reduced by TCS (Figure 9), further evidence that $IP_3$ receptor interference is not the key mechanism of TCS inhibition in T cells, as well. Instead, it is likely that TCS-induced cytosol acidification blocks the proper interaction of the STIM and ORAI1 machinery that is required for CRAC channel opening (Thompson *et al.*, 2009; Mancarella *et al.*, 2011). Histidine 155, found between transmembrane domains (TM) 2 and 3 of ORAI1, plays an important role in sensing intracellular pH (Tsujikawa *et al.*, 2015). Upon cytoplasmic acidification, histidine 155 becomes protonated and affects intermolecular interaction of other components in the loop between TM2 and TM3 of the ORAI1 that may result in CRAC channel closing (Tsujikawa *et al.*, 2015). Based upon the Henderson-Hasselbalch equation and the pKa of histidine (6.0; Nelson and Cox 2017), 5.9% of these histidines are protonated at pH 7.2, whereas 11.2% are protonated at pH 6.9. (Note: if the protein environment surrounding histidine 155 changes its pKa, there could be a greater change in its charge upon acidification). Thus, the level of acidification induced by TCS (−0.3 pH unit, Table 1) likely induces a doubling of the concentration of ORAI1 proteins containing positively-charged histidines in this key cytoplasmic motif. Regardless of the mechanism of acidification (direct injection of strong acid as in Beck *et al.*, 2014, or exposure to weak acid TCS dissolved in the extracellular buffer as in this study), the resulting acidification will cause this critical histidine to be more likely positively charged. This histidine is conserved in rat (as in RBL cells) and human (as in the Jurkat T cells), according to an NCBI Blast multiple amino acid sequence alignment. Overall, protonation and closing of CRAC channels is likely the mechanism of TCS-induced reduction of $Ca^{2+}$ influx into mast cells (Weatherly et al., 2018) and T cells (Figure 9), leading to inhibition of mast cell function (Palmer et al., 2012). Future experiments utilizing the fluorescence resonance energy

transfer techniques of Mancarella et al., 2011 or other approaches should be able to directly test the hypothesis that TCS disrupts the STIM1/ORAI1 interaction.

Future research will examine inhibition of T cell functions downstream of SOCE, such as release of essential cytokines (Punt *et al.*, 2019). In addition to the known TCS inhibition of mast cell degranulation and other functions (Palmer *et al.*, 2012), TCS also inhibits the lytic function of natural killer cells (Udoji *et al.*, 2010; Hurd-Brown *et al.*, 2013), which are important defenders against cancer and viral infections.

In addition to acidifying the cytosol by its direct proton ionophore mechanism of providing a pathway for charged protons to flow into the cell, TCS may also be acidifying the cell contents via other mechanisms. TCS increases the production of reactive oxygen species (ROS) in mast cells (Weatherly *et al.*, 2018) and in other cell types (Binelli *et al.*, 2009; Riva *et al.*, 2012; Tamura *et al.*, 2012; Yueh *et al.*, 2014; Lv *et al.*, 2016; Weatherly *et al.*, 2018), which impair the $Na/H^+$ exchanger, leading to reduced intracellular pH (Kaufman *et al.*, 1993; Nakamura *et al.*, 2006). TCS also causes mitochondrial fission/fragmentation (Weatherly *et al.*, 2018), processes associated with reduced intracellular pH as a result of lactic acid buildup attributed to increased glycolysis (Johnson and Nehrke, 2010; Schurr, 2014). While the timeframes in which these processes acidify the cell are likely longer than the rapid (within 15 min) acidification reported in this study, these mechanisms suggest that TCS will continue to acidify the cell over longer exposure times and possibly at lower doses; ROS stimulation and mitochondrial dysfunction occur in primary human keratinocytes, mast cells, and other cell types at lower doses (starting ~1 μM) than the 10–20 μM used in the current study.

If this TCS acidification occurs in the mitochondria to a similar degree (~0.3 pH unit acidification of the matrix), the driving force (Gibbs free energy) available for producing ATP on ATP synthase in the inner mitochondrial membrane will be also reduced, as previously observed (Weatherly *et al.*, 2016). This effect can be estimated by calculating the driving force both in the presence and absence of 20 μM TCS, via the equation

$$\Delta G_{\text{Transport}} = 2.3\text{RT}\Delta\text{pH} + \text{F}\Delta\Psi$$

(Nelson and Cox, 2017). Using the 37°C temperature used experimentally, the gas and Faraday's constants, $p$H = −0.75, and ΔΨ = −0.2 V (Nelson and Cox, 2017), the free energy released by protons flowing through ATP synthase into the matrix is a robust ~−24 kJ/mol in a healthy cell. Taking into account a 0.3 pH unit acidification of the matrix (such that Δ$p$H = −0.45) and a 40% reduction in ΔΨ (Weatherly *et al.*, 2018) due to 20 μM TCS exposure, the free energy released by protons flowing through ATP synthase into the matrix is a weaker ~ −14 kJ/mol in a TCS-treated cell. This result implies a ~40% reduction in the free energy available for making ATP. While imperfect, this value is a reasonable match to the >50% reduction in ATP production caused by 20 μM TCS in RBL cells (Weatherly *et al.*, 2016).

TCS inhibits MMP (Weatherly *et al.*, 2018); however, TCS does not inhibit PMP. This apparent contradiction can be explained by the inherent cellular mechanisms in charge of creating and then maintaining either the MMP or the PMP. The MMP is primarily generated

by the action of the electron transport chain (ETC) proton pumps (Nelson and Cox, 2017); MMP is entirely reliant on this segregation of protons. TCS is a proton ionophore mitochondrial uncoupler, thus, acting in direct opposition to the proton pumps of the ETC (Weatherly *et al.*, 2016). Such direct opposition, with no alternative means of MMP maintenance, serves to explain why TCS can significantly depress the MMP. In contrast to the MMP's generation by proton pumping, PMP is primarily generated by the action of the $Na^+/K^+$ ATPase, (Nelson and Cox, 2017), which is located nearly exclusively on the plasma membrane (Bertorello *et al.*, 2003) and is not present on the mitochondrial membrane. In RBL mast cells, the $Na^+/K^+$ ATPase contributes to PMP (Bronner *et al.*, 1989) and resides on the plasma membrane of RBL cells, and its inhibition leads to dampening of Ag-stimulated degranulation (Gentile and Skoner, 1996). Thus, TCS modulation of proton concentrations could affect cytosolic pH without altering PMP. TCS does cause PMP depolarization of artificial membranes which do not contain the $Na^+/K^+$ ATPase (Popova *et al.*, 2018). TCS-mediated changes in proton concentrations across these membranes would therefore not be counteracted by the $Na^+/K^+$ ATPase. TCS also causes PMP depolarization of neuronal models (Arias-Cavieres *et al.*, 2018; Popova *et al.*, 2018) at micromolar doses within tens of minutes. Neurons heavily rely on the PMP for their function and, while the $Na^+/K^+$ ATPase is still the primary source of this voltage, neurons possess additional PMP regulation mechanisms (Bean, 2007), which may explain triclosan's differential effects on PMP of immune cells vs. neuronal cells. Interestingly, TCS inhibits $Na^+/K^+$ ATPase activity in *Labeo rohita* gills (Hemalatha *et al.*, 2019), a hint that, over longer exposure periods than those used in the current study, TCS may interfere with cellular PMP.

In conclusion, we report the mechanism of TCS inhibition of mast cells and T cells (Figure 10). Three-dimensional super-resolution microscopy shows that TCS causes mitochondrial swelling in mast cells, further evidence for its depolarization of the mitochondrial membrane. However, TCS does not inhibit immune cells by dampening their plasma membrane potential. Using genetically encoded voltage indicators coupled with pH-indicating reporters, we have identified that TCS acidifies the cytosol but does not affect PMP in immune cells. Cytosolic acidification by TCS likely disrupts the Stim1-ORAI1 interaction, causing CRAC channel closing and collapse of $Ca^{2+}$ influx into mast cells and T cells. TCS-induced reduction of Ag-stimulated cytosolic $Ca^{2+}$ influx results in inhibited enzymatic activity and decreased microtubule polymerization, leading to suppression of mast cell degranulation. Collapse of SOCE in T cells also likely leads to inhibition of T cell function. Any cell type that depends on $Ca^{2+}$ signaling or mitochondrial function is susceptible to TCS toxicity (Feske, 2007; Hill-Eubanks *et al.*, 2011). In summary, TCS, a mitochondrial toxicant, is also an immunotoxicant via its modulation of immune cell signal transduction.

## Supplementary Material

Refer to Web version on PubMed Central for supplementary material.

## Acknowledgments

We thank Dr. Robert Wheeler, Siham Hattab, and Bailey Blair for use of and help with the ibidi heating system and confocal; William Simke and Andrew Hart for help with image analysis; Dr. Matthew Parent for help with 3D

imaging and analysis; Dr. Lili Wang for helpful discussions regarding imaging Jurkat T cells; and Dr. Jaime de Juan Sanz and Dr. Francois St-Pierre for helpful discussions regarding genetically encoded voltage indicators.

Funding

This research was supported by the National Institutes of Health: National Institute of Environmental Health Sciences award number R15ES24593 and National Institute of General Medical Sciences awards R15GM116002 and P20GM103423 (an Institutional Development Award) and the Maine Technological Asset Fund (MTAF 1106 and 2061). University of Maine funding that additionally supported this work includes a UMaine Medicine Seed Grant, a Charlie Slavin Research Grant, Frederick Radke Undergraduate Research Fellowships, Maine Top Scholar research supply funds, and the Center for Undergraduate Research.

## Abbreviations:

| | |
|---|---|
| **Ag** | antigen |
| **APC** | antigen presenting cell |
| **ATP** | adenosine triphosphate |
| **AUC** | area under the curve |
| **BSA** | bovine serum albumin |
| **BT** | Tyrodes-bovine serum albumin |
| **CCCP** | carbonyl cyanide 3-chlorophenylhydrazone |
| **CRAC** | $Ca^{2+}$ release-activated $Ca^{2+}$ |
| **DMSO** | dimethyl sulfoxide |
| **ER** | endoplasmic reticulum |
| **ETC** | electron transport chain |
| **FCCP** | carbonyl cyanide-p-trifluoromethoxyphenylhydrazone |
| **FPALM** | fluorescence photoactivation localization microscopy |
| **GEVI** | genetically encoded voltage indicator |
| **IgE** | immunoglobulin E |
| **$IP_3$** | inositol 1,4,5-triphosphate |
| **LDH** | lactate dehydrogenase |
| **MMP** | mitochondrial membrane potential |
| **PBS** | phosphate buffered saline |
| **$PIP_2$** | phosphatidylinositol 4,5-bisphosphate |
| **PLCγ** | phospholipase C gamma |
| **PLD** | phospholipase D |

| | |
|---|---|
| **PMP** | plasma membrane potential |
| **PSF** | point spread function |
| **RBL** | rat basophilic leukemia cells, clone 2H3 |
| **ROI** | region of interest |
| **ROS** | reactive oxygen species |
| **SEM** | standard error of the mean |
| **SOCE** | store-operated $Ca^{2+}$ entry |
| **STIM1** | stromal interaction molecule 1 |
| **TCR** | T-cell receptor |
| **TCS** | triclosan |
| **TM** | transmembrane domain |

## References


Abramson J, Pecht I, 2007 Regulation of the mast cell response to the type 1 Fc epsilon receptor. Immunol Rev 217, 231–254.10.1111/j.1600-065X.2007.00518.x [PubMed: 17498063]

Ajao C, Andersson MA, Teplova VV, Nagy S, Gahmberg CG, Andersson LC, Hautaniemi M, Kakasi B, Roivainen M, Salkinoja-Salonen M, 2015 Mitochondrial toxicity of triclosan on mammalian cells. Toxicology reports 2, 624–637.10.1016/j.toxrep.2015.03.012 [PubMed: 28962398]

Alsaleh NB, Persaud I, Brown JM, 2016 Silver Nanoparticle-Directed Mast Cell Degranulation Is Mediated through Calcium and PI3K Signaling Independent of the High Affinity IgE Receptor. PloS one 11, e0167366.10.1371/journal.pone.0167366

Anderson SE, Meade BJ, Long CM, Lukomska E, Marshall NB, 2016 Investigations of immunotoxicity and allergic potential induced by topical application of triclosan in mice. Journal of immunotoxicology 13, 165–172.10.3109/1547691x.2015.1029146 [PubMed: 25812624]

Arias-Cavieres A, More J, Vicente JM, Adasme T, Hidalgo J, Valdes JL, Humeres A, Valdes-Undurraga I, Sanchez G, Hidalgo C, Barrientos G, 2018 Triclosan Impairs Hippocampal Synaptic Plasticity and Spatial Memory in Male Rats. Front Mol Neurosci 11, 42910.3389/fnmol.2018.00429 [PubMed: 30534053]

Barrandon Y, Green H, 1985 Cell size as a determinant of the clone-forming ability of human keratinocytes. Proc Natl Acad Sci U S A 82, 5390–5394.10.1073/pnas.82.16.5390 [PubMed: 2410922]

Barros SP, Wirojchanasak S, Barrow DA, Panagakos FS, Devizio W, Offenbacher S, 2010 Triclosan inhibition of acute and chronic inflammatory gene pathways. Journal of clinical periodontology 37, 412418.10.1111/j.1600-051X.2010.01548.x

Bean BP, 2007 The action potential in mammalian central neurons. Nature reviews. Neuroscience 8, 451465.10.1038/nrn2148

Beck A, Fleig A, Penner R, Peinelt C, 2014 Regulation of endogenous and heterologous $Ca^{2+}$ release-activated $Ca^{2+}$ currents by pH. Cell calcium 56, 235–243.10.1016/j.ceca.2014.07.011 [PubMed: 25168908]

Berridge MJ, 1993 Inositol trisphosphate and calcium signalling. Nature 361, 315–325.10.1038/361315a0 [PubMed: 8381210]

Bertorello AM, Komarova Y, Smith K, Leibiger IB, Efendiev R, Pedemonte CH, Borisy G, Sznajder JI, 2003 Analysis of Na+,K+-ATPase motion and incorporation into the plasma membrane in

response to G protein-coupled receptor signals in living cells. Mol Biol Cell 14, 1149–1157.10.1091/mbc.e02-06-0367 [PubMed: 12631730]

Bhandari P, Song M, Chen Y, Burelle Y, Dorn GW 2nd, 2014 Mitochondrial contagion induced by Parkin deficiency in Drosophila hearts and its containment by suppressing mitofusin. Circulation research 114, 257–265.10.1161/circresaha.114.302734 [PubMed: 24192653]

Binelli A, Cogni D, Parolini M, Riva C, Provini A, 2009 In vivo experiments for the evaluation of genotoxic and cytotoxic effects of Triclosan in Zebra mussel hemocytes. Aquatic toxicology (Amsterdam, Netherlands) 91, 238–244.10.1016/j.aquatox.2008.11.008

Blank U, Essig M, Scandiuzzi L, Benhamou M, Kanamaru Y, 2007 Mast cells and inflammatory kidney disease. Immunol Rev 217, 79–95.10.1111/j.1600-065X.2007.00503.x [PubMed: 17498053]

Boron WF, 2004 Regulation of intracellular pH. Advances in physiology education 28, 160–179.10.1152/advan.00045.2004 [PubMed: 15545345]

Bronner C, Mousli M, Eleno N, Landry Y, 1989 Resting plasma membrane potential of rat peritoneal mast cells is set predominantly by the sodium pump. FEBS letters 255, 401–404.10.1016/00145793(89)81132-9 [PubMed: 2477283]

Cai S, Zhu J, Sun L, Fan C, Zhong Y, Shen Q, Li Y, 2019 Association Between Urinary Triclosan With Bone Mass Density and Osteoporosis in US Adult Women, 2005−2010. The Journal of clinical endocrinology and metabolism 104, 4531–4538.10.1210/jc.2019-00576 [PubMed: 31237619]

Calafat AM, Ye X, Wong LY, Reidy JA, Needham LL, 2008 Urinary concentrations of triclosan in the U.S. population: 2003–2004. Environmental health perspectives 116, 303–307.10.1289/ehp.10768 [PubMed: 18335095]

Chahdi A, Choi WS, Kim YM, Fraundorfer PF, Beaven MA, 2002 Serine/threonine protein kinases synergistically regulate phospholipase D1 and 2 and secretion in RBL-2H3 mast cells. Mol Immunol 38, 1269–1276.10.1016/s0161-5890(02)00074-3 [PubMed: 12217394]

Chalfie M, Kain S, 2005 Green Fluorescent Protein: Properties, Applications and Protocols. John Wiley & Sons.

Chamberland S, Yang HH, Pan MM, Evans SW, Guan S, Chavarha M, Yang Y, Salesse C, Wu H, Wu JC, Clandinin TR, Toth K, Lin MZ, St-Pierre F, 2017 Fast two-photon imaging of subcellular voltage dynamics in neuronal tissue with genetically encoded indicators. Elife 6, e25690.10.7554/eLife.25690

Chandra S, Fewtrell C, Millard PJ, Sandison DR, Webb WW, Morrison GH, 1994 Imaging of total intracellular calcium and calcium influx and efflux in individual resting and stimulated tumor mast cells using ion microscopy. J Biol Chem 269, 15186–15194 [PubMed: 8195154]

Chen H, Detmer SA, Ewald AJ, Griffin EE, Fraser SE, Chan DC, 2003 Mitofusins Mfn1 and Mfn2 coordinately regulate mitochondrial fusion and are essential for embryonic development. J Cell Biol 160, 189–200.10.1083/jcb.200211046 [PubMed: 12527753]

Chen TW, Wardill TJ, Sun Y, Pulver SR, Renninger SL, Baohan A, Schreiter ER, Kerr RA, Orger MB, Jayaraman V, Looger LL, Svoboda K, Kim DS, 2013 Ultrasensitive fluorescent proteins for imaging neuronal activity. Nature 499, 295–300.10.1038/nature12354 [PubMed: 23868258]

Compan V, Baroja-Mazo A, López-Castejón G, Gomez AI, Martínez CM, Angosto D, Montero MT, Herranz AS, Bazán E, Reimers D, Mulero V, Pelegrín P, 2012 Cell volume regulation modulates NLRP3 inflammasome activation. Immunity 37, 487–500.10.1016/j.immuni.2012.06.013 [PubMed: 22981536]

Cui M, Tang X, Christian WV, Yoon Y, Tieu K, 2010 Perturbations in mitochondrial dynamics induced by human mutant PINK1 can be rescued by the mitochondrial division inhibitor mdivi-1. J Biol Chem 285, 11740–11752.10.1074/jbc.M109.066662 [PubMed: 20164189]

Curthoys NM, Mlodzianoski MJ, Parent M, Butler MB, Raut P, Wallace J, Lilieholm J, Mehmood K, Maginnis MS, Waters H, Busse B, Zimmerberg J, Hess ST, 2019 Influenza Hemagglutinin Modulates Phosphatidylinositol 4,5-Bisphosphate Membrane Clustering. Biophys J 116, 893909.10.1016/j.bpj.2019.01.017

Daoud FC, Edmiston CE Jr., Leaper D, 2014 Meta-analysis of prevention of surgical site infections following incision closure with triclosan-coated sutures: robustness to new evidence. Surgical infections 15, 165–181.10.1089/sur.2013.177 [PubMed: 24738988]

Dvorak AM, 1986 Mast-cell degranulation in human hearts. The New England journal of medicine 315, 969–970.10.1056/nejm198610093151515

Elieh-Ali-Komi D, Cao Y, 2017 Role of Mast Cells in the Pathogenesis of Multiple Sclerosis and Experimental Autoimmune Encephalomyelitis. Clinical reviews in allergy & immunology 52, 436–445.10.1007/s12016-016-8595-y [PubMed: 28025778]

Etzel TM, Calafat AM, Ye X, Chen A, Lanphear BP, Savitz DA, Yolton K, Braun JM, 2017 Urinary triclosan concentrations during pregnancy and birth outcomes. Environmental research 156, 505–511.10.1016/j.envres.2017.04.015 [PubMed: 28427038]

Farrell DJ, Hines JE, Walls AF, Kelly PJ, Bennett MK, Burt AD, 1995 Intrahepatic mast cells in chronic liver diseases. Hepatology (Baltimore, Md.) 22, 1175–1181.10.1016/0270-9139(95)90627-4

Feske S, 2007 Calcium signalling in lymphocyte activation and disease. Nature reviews. Immunology 7, 690–702.10.1038/nri2152

Fewtrell C, Geier M, Goetze A, Holowka D, Isenman DE, Jones JF, Metzger H, Navia M, Sieckmann D, Silverton E, Stein K, 1979 Mediation of effector functions by antibodies: report of a workshop. Mol Immunol 16, 741–754.10.1016/0161-5890(79)90152-4 [PubMed: 521049]

Galli SJ, Kalesnikoff J, Grimbaldeston MA, Piliponsky AM, Williams CM, Tsai M, 2005 Mast cells as “tunable” effector and immunoregulatory cells: recent advances. Annual review of immunology 23, 749–786.10.1146/annurev.immunol.21.120601.141025

Gentile DA, Skoner DP, 1996 A role for the sodium, potassium adenosine triphosphatase (Na+,K+ ATPase) enzyme in degranulation of rat basophilic leukaemia cells. Clinical and experimental allergy : journal of the British Society for Allergy and Clinical Immunology 26, 1449–1460 [PubMed: 9027446]

Giedt RJ, Pfeiffer DR, Matzavinos A, Kao CY, Alevriadou BR, 2012 Mitochondrial dynamics and motility inside living vascular endothelial cells: role of bioenergetics. Annals of biomedical engineering 40, 1903–1916.10.1007/s10439-012-0568-6 [PubMed: 22527011]

Gilbert RJ, 1987 The oral clearance of zinc and triclosan after delivery from a dentifrice. J Pharm Pharmacol 39, 480–483.10.1111/j.2042-7158.1987.tb03425.x [PubMed: 2886608]

Girolamo F, Coppola C, Ribatti D, 2017 Immunoregulatory effect of mast cells influenced by microbes in neurodegenerative diseases. Brain, behavior, and immunity 65, 68–89.10.1016/j.bbi.2017.06.017

Gottlieb S, 2019Federal register. Vol.84 (71): https://www.govinfo.gov/content/pkg/FR-2019-04-12/pdf/2019-06791.pdf

Gudheti MV, Curthoys NM, Gould TJ, Kim D, Gunewardene MS, Gabor KA, Gosse JA, Kim CH, Zimmerberg J, Hess ST, 2013 Actin mediates the nanoscale membrane organization of the clustered membrane protein influenza hemagglutinin. Biophys J 104, 2182–2192.10.1016/j.bpj.2013.03.054 [PubMed: 23708358]

Guillery O, Malka F, Frachon P, Milea D, Rojo M, Lombès A, 2008 Modulation of mitochondrial morphology by bioenergetics defects in primary human fibroblasts. Neuromuscular disorders : NMD 18, 319–330.10.1016/j.nmd.2007.12.008 [PubMed: 18395446]

Guo Z, Turner C, Castle D, 1998 Relocation of the t-SNARE SNAP-23 from lamellipodia-like cell surface projections regulates compound exocytosis in mast cells. Cell 94, 537–548.10.1016/s0092-8674(00)81594-9 [PubMed: 9727496]

Hara Y, Yuk F, Puri R, Janssen WG, Rapp PR, Morrison JH, 2014 Presynaptic mitochondrial morphology in monkey prefrontal cortex correlates with working memory and is improved with estrogen treatment. Proc Natl Acad Sci U S A 111, 486–491.10.1073/pnas.1311310110 [PubMed: 24297907]

Hemalatha D, Nataraj B, Rangasamy B, Shobana C, Ramesh M, 2019 DNA damage and physiological responses in an Indian major carp Labeo rohita exposed to an antimicrobial agent triclosan. Fish physiology and biochemistry 45, 1463–1484.10.1007/s10695-019-00661-2 [PubMed: 31222661]

Hempel HA, Cuka NS, Kulac I, Barber JR, Cornish TC, Platz EA, De Marzo AM, Sfanos KS, 2017 Low Intratumoral Mast Cells Are Associated With a Higher Risk of Prostate Cancer Recurrence. The Prostate 77, 412–424.10.1002/pros.23280 [PubMed: 27868214]

Hess ST, Girirajan TP, Mason MD, 2006 Ultra-high resolution imaging by fluorescence photoactivation localization microscopy. Biophys J 91, 4258–4272.10.1529/biophysj.106.091116 [PubMed: 16980368]

Hill-Eubanks DC, Werner ME, Heppner TJ, Nelson MT, 2011 Calcium signaling in smooth muscle. Cold Spring Harbor perspectives in biology 3, a004549.10.1101/cshperspect.a004549

Hogan PG, Lewis RS, Rao A, 2010 Molecular basis of calcium signaling in lymphocytes: STIM and ORAI. Annual review of immunology 28, 491–533.10.1146/annurev.immunol.021908.132550

Holowka D, Calloway N, Cohen R, Gadi D, Lee J, Smith NL, Baird B, 2012 Roles for ca(2+) mobilization and its regulation in mast cell functions. Front Immunol 3, 10410.3389/fimmu.2012.00104 [PubMed: 22586429]

Holowka D, Thanapuasuwan K, Baird B, 2018 Short chain ceramides disrupt immunoreceptor signaling by inhibiting segregation of Lo from Ld Plasma membrane components. Biol Open 710.1242/bio.034702

Huang B, Wang W, Bates M, Zhuang X, 2008 Three-dimensional super-resolution imaging by stochastic optical reconstruction microscopy. Science 319, 810–813.10.1126/science.1153529 [PubMed: 18174397]

Hurd-Brown T, Udoji F, Martin T, Whalen MM, 2013 Effects of DDT and triclosan on tumor-cell binding capacity and cell-surface protein expression of human natural killer cells. J Appl Toxicol 33, 495–502.10.1002/jat.2767 [PubMed: 22729613]

Hutchinson LM, Trinh BM, Palmer RK, Preziosi CA, Pelletier JH, Nelson HM, Gosse JA, 2011 Inorganic arsenite inhibits IgE receptor-mediated degranulation of mast cells. J Appl Toxicol 31, 231–241.10.1002/jat.1585 [PubMed: 20842677]

Jackson-Browne MS, Papandonatos GD, Chen A, Calafat AM, Yolton K, Lanphear BP, Braun JM, 2018 Identifying Vulnerable Periods of Neurotoxicity to Triclosan Exposure in Children. Environmental health perspectives 126, 057001.10.1289/ehp2777

Jackson-Browne MS, Papandonatos GD, Chen A, Yolton K, Lanphear BP, Braun JM, 2019 Early-life triclosan exposure and parent-reported behavior problems in 8-year-old children. Environment international 128, 446–456.10.1016/j.envint.2019.01.021 [PubMed: 30712883]

Jheng HF, Tsai PJ, Guo SM, Kuo LH, Chang CS, Su IJ, Chang CR, Tsai YS, 2012 Mitochondrial fission contributes to mitochondrial dysfunction and insulin resistance in skeletal muscle. Molecular and cellular biology 32, 309–319.10.1128/mcb.05603-11 [PubMed: 22083962]

Jin L, Han Z, Platisa J, Wooltorton JR, Cohen LB, Pieribone VA, 2012 Single action potentials and subthreshold electrical events imaged in neurons with a fluorescent protein voltage probe. Neuron 75, 779–785.10.1016/j.neuron.2012.06.040 [PubMed: 22958819]

Johnson D, Nehrke K, 2010 Mitochondrial fragmentation leads to intracellular acidification in Caenorhabditis elegans and mammalian cells. Mol Biol Cell 21, 2191–2201.10.1091/mbc.e09-10-0874 [PubMed: 20444981]

Johnson RG, Carty SE, Fingerhood BJ, Scarpa A, 1980 The internal pH of mast cell granules. FEBS letters 120, 75–79.10.1016/0014-5793(80)81050-7 [PubMed: 7002612]

Johnzon CF, Rönnberg E, Pejler G, 2016 The Role of Mast Cells in Bacterial Infection. The American journal of pathology 186, 4–14.10.1016/j.ajpath.2015.06.024 [PubMed: 26477818]

Jurewicz J, Radwan M, Wielgomas B, Kałużny P, Klimowska A, Radwan P, Hanke W, 2018 Environmental levels of triclosan and male fertility. Environmental science and pollution research international 25, 5484–5490.10.1007/s11356-017-0866-5 [PubMed: 29214481]

Kary T, 2019 Colgate Total Toothpaste to Relaunch Without Controversial Chemical. Bloomberg 6 19, 2020,https://www.bloomberg.com/news/articles/2019-01-15/colgate-total-toothpaste-to-relaunch-this-time-sans-triclosan

Kaufman DS, Goligorsky MS, Nord EP, Graber ML, 1993 Perturbation of cell pH regulation by H2O2 in renal epithelial cells. Archives of biochemistry and biophysics 302, 245–254.10.1006/abbi.1993.1206 [PubMed: 7682391]

Kim J, Kim K, 2019 Association of antimicrobial household exposure with development of allergic rhinitis in Korea. Pediatric allergy and immunology : official publication of the European Society of Pediatric Allergy and Immunology 30, 569–571.10.1111/pai.13052 [PubMed: 30861215]

Kinet JP, 1999 The high-affinity IgE receptor (Fc epsilon RI): from physiology to pathology. Annual review of immunology 17, 931–972.10.1146/annurev.immunol.17.1.931

Koeppe ES, Ferguson KK, Colacino JA, Meeker JD, 2013 Relationship between urinary triclosan and paraben concentrations and serum thyroid measures in NHANES 2007–2008. The Science of the total environment 445–446, 299–305.10.1016/j.scitotenv.2012.12.052

Koivusalo M, Welch C, Hayashi H, Scott CC, Kim M, Alexander T, Touret N, Hahn KM, Grinstein S, 2010 Amiloride inhibits macropinocytosis by lowering submembranous pH and preventing Rac1 and Cdc42 signaling. J Cell Biol 188, 547–563.10.1083/jcb.200908086 [PubMed: 20156964]

Kostyuk AI, Demidovich AD, Kotova DA, Belousov VV, Bilan DS, 2019 Circularly Permuted Fluorescent Protein-Based Indicators: History, Principles, and Classification. International journal of molecular sciences 20, 420010.3390/ijms20174200

Kux L, 2016Federal register. Vol.81 (126): https://www.govinfo.gov/content/pkg/FR-2016-06-30/pdf/2016-15410.pdf

Kux L, 2017Federal register. Vol.82 (243): https://www.govinfo.gov/content/pkg/FR-2017-12-20/pdf/2017-27317.pdf

Lee J, Veatch SL, Baird B, Holowka D, 2012 Molecular mechanisms of spontaneous and directed mast cell motility. J Leukoc Biol 92, 1029–1041.10.1189/jlb.0212091 [PubMed: 22859829]

Lindau M, Fernandez JM, 1986 A patch-clamp study of histamine-secreting cells. J Gen Physiol 88, 349–368.10.1085/jgp.88.3.349 [PubMed: 2428921]

Lodish H, Berk A, Zipursky SL, Matsudaira P, Baltimore D, Darnell J, 2000 Molecular Cell Biology, 4th ed W.H. Freeman.

Luby-Phelps K, 2000 Cytoarchitecture and physical properties of cytoplasm: volume, viscosity, diffusion, intracellular surface area. International review of cytology 192, 189–221.10.1016/s0074-7696(08)60527-6 [PubMed: 10553280]

Lv Y, Rui C, Dai Y, Pang Q, Li Y, Fan R, Lu S, 2016 Exposure of children to BPA through dust and the association of urinary BPA and triclosan with oxidative stress in Guangzhou, China. Environmental science. Processes & impacts 18, 1492–1499.10.1039/c6em00472e [PubMed: 27808329]

Mancarella S, Wang Y, Deng X, Landesberg G, Scalia R, Panettieri RA, Mallilankaraman K, Tang XD, Madesh M, Gill DL, 2011 Hypoxia-induced acidosis uncouples the STIM-Orai calcium signaling complex. J Biol Chem 286, 44788–44798.10.1074/jbc.M111.303081 [PubMed: 22084246]

Marano N, Liotta MA, Slattery JP, Holowka D, Baird B, 1993 Fc epsilon RI and the T cell receptor for antigen activate similar signalling pathways in T cell-RBL cell hybrids. Cell Signal 5, 155–167.10.1016/0898-6568(93)90067-v [PubMed: 8499225]

Marshall NB, Lukomska E, Long CM, Kashon ML, Sharpnack DD, Nayak AP, Anderson KL, Jean Meade B, Anderson SE, 2015 Triclosan Induces Thymic Stromal Lymphopoietin in Skin Promoting Th2 Allergic Responses. Toxicol Sci 147, 127–139.10.1093/toxsci/kfv113 [PubMed: 26048654]

Marshall NB, Lukomska E, Nayak AP, Long CM, Hettick JM, Anderson SE, 2017 Topical application of the anti-microbial chemical triclosan induces immunomodulatory responses through the S100A8/A9-TLR4 pathway. Journal of immunotoxicology 14, 50–59.10.1080/1547691x.2016.1258094 [PubMed: 28121465]

McLaughlin SG, Dilger JP, 1980 Transport of protons across membranes by weak acids. Physiological reviews 60, 825–863.10.1152/physrev.1980.60.3.825 [PubMed: 6248908]

Metcalfe DD, Baram D, Mekori YA, 1997 Mast cells. Physiological reviews 77, 1033–1079.10.1152/physrev.1997.77.4.1033 [PubMed: 9354811]

Metzger H, Goetze A, Kanellopoulos J, Holowka D, Fewtrell C, 1982 Structure of the high-affinity mast cell receptor for IgE. Fed Proc 41, 8–11 [PubMed: 6459957]

Millard PJ, Gross D, Webb WW, Fewtrell C, 1988 Imaging asynchronous changes in intracellular Ca2+ in individual stimulated tumor mast cells. Proc Natl Acad Sci U S A 85, 1854–1858.10.1073/pnas.85.6.1854 [PubMed: 3162312]

Miyawaki A, Niino Y, 2015 Molecular spies for bioimaging--fluorescent protein-based probes. Molecular cell 58, 632–643.10.1016/j.molcel.2015.03.002 [PubMed: 26000848]

Mohr FC, Fewtrell C, 1987a Depolarization of rat basophilic leukemia cells inhibits calcium uptake and exocytosis. J Cell Biol 104, 783–792.10.1083/jcb.104.3.783 [PubMed: 2950123]

Mohr FC, Fewtrell C, 1987b The relative contributions of extracellular and intracellular calcium to secretion from tumor mast cells. Multiple effects of the proton ionophore carbonyl cyanide m-chlorophenylhydrazone. J Biol Chem 262, 10638–10643 [PubMed: 2440869]

Moss T, Howes D, Williams FM, 2000 Percutaneous penetration and dermal metabolism of triclosan (2,4, 4'-trichloro-2'-hydroxydiphenyl ether). Food and chemical toxicology : an international journal published for the British Industrial Biological Research Association 38, 361–370.10.1016/s0278-6915(99)00164-7 [PubMed: 10722890]

Myers VB, Haydon DA, 1972 Ion transfer across lipid membranes in the presence of gramicidin A. II. The ion selectivity. Biochim Biophys Acta 274, 313–322.10.1016/0005-2736(72)90179-4 [PubMed: 5049000]

Nakamura U, Iwase M, Uchizono Y, Sonoki K, Sasaki N, Imoto H, Goto D, Iida M, 2006 Rapid intracellular acidification and cell death by H2O2 and alloxan in pancreatic beta cells. Free radical biology & medicine 40, 2047–2055.10.1016/j.freeradbiomed.2006.01.038 [PubMed: 16716905]

Nelson DL, Cox MM, 2017 Lehninger Principles of Biochemistry, 7th ed W.H. Freeman.

Ouyang F, Tang N, Zhang HJ, Wang X, Zhao S, Wang W, Zhang J, Cheng W, 2018 Maternal urinary triclosan level, gestational diabetes mellitus and birth weight in Chinese women. The Science of the total environment 626, 451–457.10.1016/j.scitotenv.2018.01.102 [PubMed: 29353787]

Ozawa K, Yamada K, Kazanietz MG, Blumberg PM, Beaven MA, 1993 Different isozymes of protein kinase C mediate feedback inhibition of phospholipase C and stimulatory signals for exocytosis in rat RBL-2H3 cells. J Biol Chem 268, 2280–2283 [PubMed: 8381401]

Palmer RK, Hutchinson LM, Burpee BT, Tupper EJ, Pelletier JH, Kormendy Z, Hopke AR, Malay ET, Evans BL, Velez A, Gosse JA, 2012 Antibacterial agent triclosan suppresses RBL-2H3 mast cell function. Toxicol Appl Pharmacol 258, 99–108.10.1016/j.taap.2011.10.012 [PubMed: 22036726]

Parent M, Hess ST, 2019 Quantification of Mitochondrial Membrane Curvature by Three-Dimensional Localization Microscopy. iScience Notes 410.22580

Popova LB, Nosikova ES, Kotova EA, Tarasova EO, Nazarov PA, Khailova LS, Balezina OP, Antonenko YN, 2018 Protonophoric action of triclosan causes calcium efflux from mitochondria, plasma membrane depolarization and bursts of miniature end-plate potentials. Biochim Biophys Acta Biomembr 1860, 1000–1007.10.1016/j.bbamem.2018.01.008 [PubMed: 29317196]

Prakriya M, Lewis RS, 2015 Store-Operated Calcium Channels. Physiological reviews 95, 1383–1436.10.1152/physrev.00020.2014 [PubMed: 26400989]

Punt J, Stranford S, Jones P, Owen J, 2019 Kuby Immunology, 8th ed W.H. Freeman.

Putney JW Jr., 1986 A model for receptor-regulated calcium entry. Cell calcium 7, 1–12.10.1016/0143-4160(86)90026-6 [PubMed: 2420465]

Queckenberg C, Meins J, Wachall B, Doroshyenko O, Tomalik-Scharte D, Bastian B, Abdel-Tawab M, Fuhr U, 2010 Absorption, pharmacokinetics, and safety of triclosan after dermal administration. Antimicrob Agents Chemother 54, 570–572.10.1128/aac.00615-09 [PubMed: 19822703]

Riva C, Cristoni S, Binelli A, 2012 Effects of triclosan in the freshwater mussel Dreissena polymorpha: a proteomic investigation. Aquatic toxicology (Amsterdam, Netherlands) 118–119, 62–71.10.1016/j.aquatox.2012.03.013

Rover JA, Leu-Wai-See P, 2014 Role of Colgate Total toothpaste in helping control plaque and gingivitis. American journal of dentistry 27, 167–170 [PubMed: 25208366]

Safiulina D, Veksler V, Zharkovsky A, Kaasik A, 2006 Loss of mitochondrial membrane potential is associated with increase in mitochondrial volume: physiological role in neurones. J Cell Physiol 206, 347–353.10.1002/jcp.20476 [PubMed: 16110491]

Sarkadi B, Tordai A, Gardos G, 1990 Membrane depolarization selectively inhibits receptor-operated calcium channels in human T (Jurkat) lymphoblasts. Biochim Biophys Acta 1027, 130–140.10.1016/0005-2736(90)90076-z [PubMed: 2168754]

Schurr A, 2014 Cerebral glycolysis: a century of persistent misunderstanding and misconception. Frontiers in neuroscience 8, 36010.3389/fnins.2014.00360 [PubMed: 25477776]

Seldin DC, Adelman S, Austen KF, Stevens RL, Hein A, Caulfield JP, Woodbury RG, 1985 Homology of the rat basophilic leukemia cell and the rat mucosal mast cell. Proc Natl Acad Sci U S A 82, 3871–3875.10.1073/pnas.82.11.3871 [PubMed: 3923482]

Shim J, Weatherly LM, Luc RH, Dorman MT, Neilson A, Ng R, Kim CH, Millard PJ, Gosse JA, 2016 Triclosan is a mitochondrial uncoupler in live zebrafish. J Appl Toxicol 36, 1662–1667.10.1002/jat.3311 [PubMed: 27111768]

Shim JK, Caron MA, Weatherly LM, Gerchman LB, Sangroula S, Hattab S, Baez AY, Briana TJ, Gosse JA, 2019 Antimicrobial agent triclosan suppresses mast cell signaling via phospholipase D inhibition. J Appl Toxicol 39, 1672–1690.10.1002/jat.3884 [PubMed: 31429102]

Silver R, Curley JP, 2013 Mast cells on the mind: new insights and opportunities. Trends in neurosciences 36, 513–521.10.1016/j.tins.2013.06.001 [PubMed: 23845731]

Smith AJ, Pfeiffer JR, Zhang J, Martinez AM, Griffiths GM, Wilson BS, 2003 Microtubule-dependent transport of secretory vesicles in RBL-2H3 cells. Traffic 4, 302–312.10.1034/j.1600-0854.2003.00084.x [PubMed: 12713658]

Sneath PH, 1957 The application of computers to taxonomy. Journal of general microbiology 17, 201–226.10.1099/00221287-17-1-201 [PubMed: 13475686]

Sporik R, Kemp AS, 1997 Topical triclosan treatment of atopic dermatitis. The Journal of allergy and clinical immunology 99, 86110.1016/s0091-6749(97)80029-2

Stepanenko OV, Verkhusha VV, Kuznetsova IM, Uversky VN, Turoverov KK, 2008 Fluorescent proteins as biomarkers and biosensors: throwing color lights on molecular and cellular processes. Current protein & peptide science 9, 338–369.10.2174/138920308785132668 [PubMed: 18691124]

Tamura I, Kanbara Y, Saito M, Horimoto K, Satoh M, Yamamoto H, Oyama Y, 2012 Triclosan, an antibacterial agent, increases intracellular Zn(2+) concentration in rat thymocytes: its relation to oxidative stress. Chemosphere 86, 70–75.10.1016/j.chemosphere.2011.09.009 [PubMed: 22000841]

Tan WP, Suresh S, Tey HL, Chiam LY, Goon AT, 2010 A randomized double-blind controlled trial to compare a triclosan-containing emollient with vehicle for the treatment of atopic dermatitis. Clinical and experimental dermatology 35, e109–112.10.1111/j.1365-2230.2009.03719.x [PubMed: 19843084]

Te Winkel JD, Gray DA, Seistrup KH, Hamoen LW, Strahl H, 2016 Analysis of Antimicrobial-Triggered Membrane Depolarization Using Voltage Sensitive Dyes. Front Cell Dev Biol 4, 2910.3389/fcell.2016.00029 [PubMed: 27148531]

Theoharides TC, Sant GR, 1991 Bladder mast cell activation in interstitial cystitis. Seminars in urology 9, 74–87 [PubMed: 1853017]

Thompson MA, Pabelick CM, Prakash YS, 2009 Role of STIM1 in regulation of store-operated Ca2+ influx in pheochromocytoma cells. Cellular and molecular neurobiology 29, 193–202.10.1007/s10571-008-9311-0 [PubMed: 18807171]

Thrasher SM, Scalfone LK, Holowka D, Appleton JA, 2013 In vitro modelling of rat mucosal mast cell function in Trichinella spiralis infection. Parasite Immunol 35, 21–31.10.1111/pim.12014 [PubMed: 23094823]

Trebak M, Kinet JP, 2019 Calcium signalling in T cells. Nature reviews. Immunology 19, 154–169.10.1038/s41577-018-0110-7

Tretter L, Chinopoulos C, Adam-Vizi V, 1998 Plasma membrane depolarization and disturbed Na+ homeostasis induced by the protonophore carbonyl cyanide-p-trifluoromethoxyphenyl-hydrazon in isolated nerve terminals. Mol Pharmacol 53, 734–741.10.1124/mol.53.4.734 [PubMed: 9547365]

Tsujikawa H, Yu AS, Xie J, Yue Z, Yang W, He Y, Yue L, 2015 Identification of key amino acid residues responsible for internal and external pH sensitivity of Orai1/STIM1 channels. Sci Rep 5, 1674710.1038/srep16747 [PubMed: 26576490]

Tsukioka M, Iino M, Endo M, 1994 pH dependence of inositol 1,4,5-trisphosphate-induced Ca2+ release in permeabilized smooth muscle cells of the guinea-pig. The Journal of physiology 475, 369–375.10.1113/jphysiol.1994.sp020078 [PubMed: 8006822]

Udoji F, Martin T, Etherton R, Whalen MM, 2010 Immunosuppressive effects of triclosan, nonylphenol, and DDT on human natural killer cells in vitro. Journal of immunotoxicology 7, 205–212.10.3109/15476911003667470 [PubMed: 20297919]

Vélez MP, Arbuckle TE, Fraser WD, 2015 Female exposure to phenols and phthalates and time to pregnancy: the Maternal-Infant Research on Environmental Chemicals (MIREC) Study. Fertility and sterility 103, 1011–1020.e1012.10.1016/j.fertnstert.2015.01.005 [PubMed: 25681860]

Vig M, Beck A, Billingsley JM, Lis A, Parvez S, Peinelt C, Koomoa DL, Soboloff J, Gill DL, Fleig A, Kinet JP, Penner R, 2006 CRACM1 multimers form the ion-selective pore of the CRAC channel. Current biology : CB 16, 2073–2079.10.1016/j.cub.2006.08.085 [PubMed: 16978865]

Wang L, Izadmehr S, Kamau E, Kong XP, Chen BK, 2019 Sequential trafficking of Env and Gag to HIV-1 T cell virological synapses revealed by live imaging. Retrovirology 16, 210.1186/s12977-019-0464-3 [PubMed: 30646921]

Wang X, Chen X, Feng X, Chang F, Chen M, Xia Y, Chen L, 2015 Triclosan causes spontaneous abortion accompanied by decline of estrogen sulfotransferase activity in humans and mice. Sci Rep 5, 1825210.1038/srep18252 [PubMed: 26666354]

Wang X, Ouyang F, Feng L, Wang X, Liu Z, Zhang J, 2017 Maternal Urinary Triclosan Concentration in Relation to Maternal and Neonatal Thyroid Hormone Levels: A Prospective Study. Environmental health perspectives 125, 067017.10.1289/ehp500

Weatherly LMMolecular Mechanisms Underlying Effects of Antibacterial Agent Triclosan on Cellular Signal Transduction and Mitochondrial Function(2017). Electronic Theses and Dissertations https://digitalcommons.library.umaine.edu/etd/2727/

Weatherly LM, Gosse JA, 2017 Triclosan exposure, transformation, and human health effects. Journal of toxicology and environmental health. Part B, Critical reviews 20, 447–469.10.1080/10937404.2017.1399306

Weatherly LM, Kennedy RH, Shim J, Gosse JA, 2013 A microplate assay to assess chemical effects on RBL-2H3 mast cell degranulation: effects of triclosan without use of an organic solvent. Journal of visualized experiments : JoVE, e50671.10.3791/50671

Weatherly LM, Nelson AJ, Shim J, Riitano AM, Gerson ED, Hart AJ, de Juan-Sanz J, Ryan TA, Sher R, Hess ST, Gosse JA, 2018 Antimicrobial agent triclosan disrupts mitochondrial structure, revealed by super-resolution microscopy, and inhibits mast cell signaling via calcium modulation. Toxicol Appl Pharmacol 349, 39–54.10.1016/j.taap.2018.04.005 [PubMed: 29630968]

Weatherly LM, Shane HL, Friend SA, Lukomska E, Baur R, Anderson SE, 2020 Topical application of the antimicrobial agent triclosan induces NLRP3 inflammasome activation and mitochondrial dysfunction. Toxicol Sci.10.1093/toxsci/kfaa056

Weatherly LM, Shim J, Hashmi HN, Kennedy RH, Hess ST, Gosse JA, 2016 Antimicrobial agent triclosan is a proton ionophore uncoupler of mitochondria in living rat and human mast cells and in primary human keratinocytes. J Appl Toxicol 36, 777–789.10.1002/jat.3209 [PubMed: 26204821]

Wischmeyer E, Lentes KU, Karschin A, 1995 Physiological and molecular characterization of an IRK-type inward rectifier K+ channel in a tumour mast cell line. Pflugers Arch 429, 809–819 [PubMed: 7603835]

Xie X, Lu C, Wu M, Liang J, Ying Y, Liu K, Huang X, Zheng S, Du X, Liu D, Wen Z, Hao G, Yang G, Feng L, Jing C, 2020 Association between triclocarban and triclosan exposures and the risks of type 2 diabetes mellitus and impaired glucose tolerance in the National Health and Nutrition Examination Survey (NHANES 2013–2014). Environment international 136, 105445.10.1016/j.envint.2019.105445

Yueh MF, Taniguchi K, Chen S, Evans RM, Hammock BD, Karin M, Tukey RH, 2014 The commonly used antimicrobial additive triclosan is a liver tumor promoter. Proc Natl Acad Sci U S A 111, 17200–17205.10.1073/pnas.1419119111 [PubMed: 25404284]

Zaitsu M, Narita S, Lambert KC, Grady JJ, Estes DM, Curran EM, Brooks EG, Watson CS, Goldblum RM, Midoro-Horiuti T, 2007 Estradiol activates mast cells via a non-genomic estrogen receptor-alpha and calcium influx. Mol Immunol 44, 1977–1985.10.1016/j.molimm.2006.09.030 [PubMed: 17084457]

Zamkowska D, Karwacka A, Jurewicz J, Radwan M, 2018 Environmental exposure to non-persistent endocrine disrupting chemicals and semen quality: An overview of the current epidemiological evidence. International journal of occupational medicine and environmental health 31, 377–414.10.13075/ijomeh.1896.01195 [PubMed: 30160090]

Zhu W, Zhou W, Huo X, Zhao S, Gan Y, Wang B, Cheng W, Ouyang F, Wang W, Tian Y, Zhang J, 2019 Triclosan and Female Reproductive Health: A Preconceptional Cohort Study. Epidemiology (Cambridge, Mass.) 30 Suppl 1, S24–s31.10.1097/ede.0000000000001011

- Antimicrobial triclosan inhibits mast cell and T cell signal transduction
- Three-dimensional super-resolution microscopy reveals mitochondrial swelling
- Triclosan inhibits crosslinker-stimulated $Ca^{2+}$ influx into mast cells and T cells
- Triclosan does not affect plasma membrane potential in mast cells and T cells
- Triclosan acidifies the cytosol, thus impairing plasma membrane $Ca^{2+}$ channels

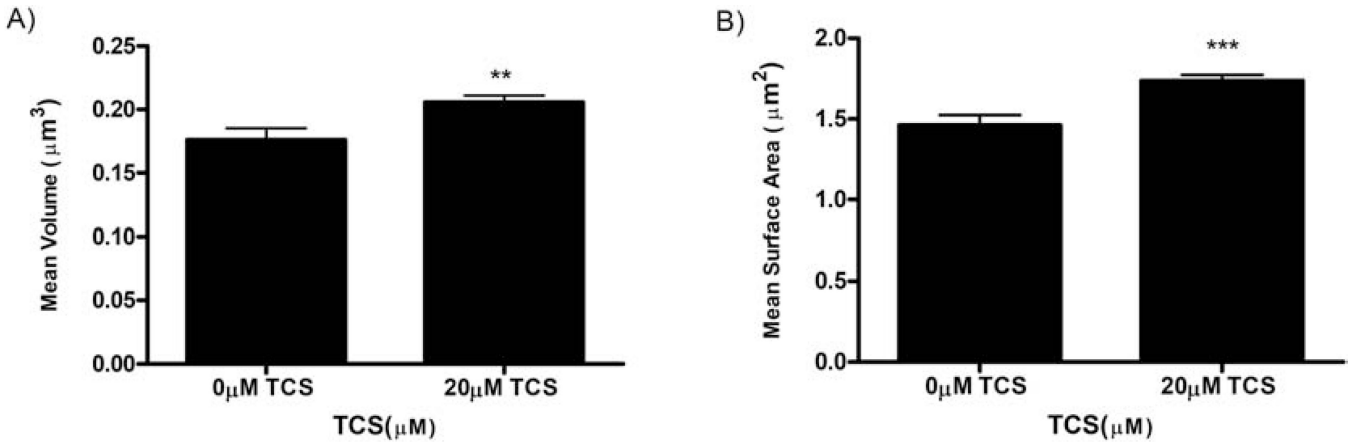


**Figure 1.**

Triclosan effects on mitochondrial volume and surface area in RBL mast cells. Super-resolution FPALM 3D images of Dendra2-TOM20, which labels outer mitochondrial membranes, were processed through custom-built MATLAB code in which an algorithm identifies individual mitochondria. As detailed in the Methods, (A) average mitochondrial volume was calculated by the convex hull method, and (B) average mitochondrial surface area was calculated by the alpha shape method. Values presented are mean SEM for total of 62 cells in three independent experiments, where each independent experiment had 8–11 cells for each condition (0 vs. 20 μM triclosan). Statistically significant results are represented by **$p<0.01$ and ***$p<0.001$ as compared to control (0 μM TCS) for volume and surface area, respectively, as determined by unpaired t-test.

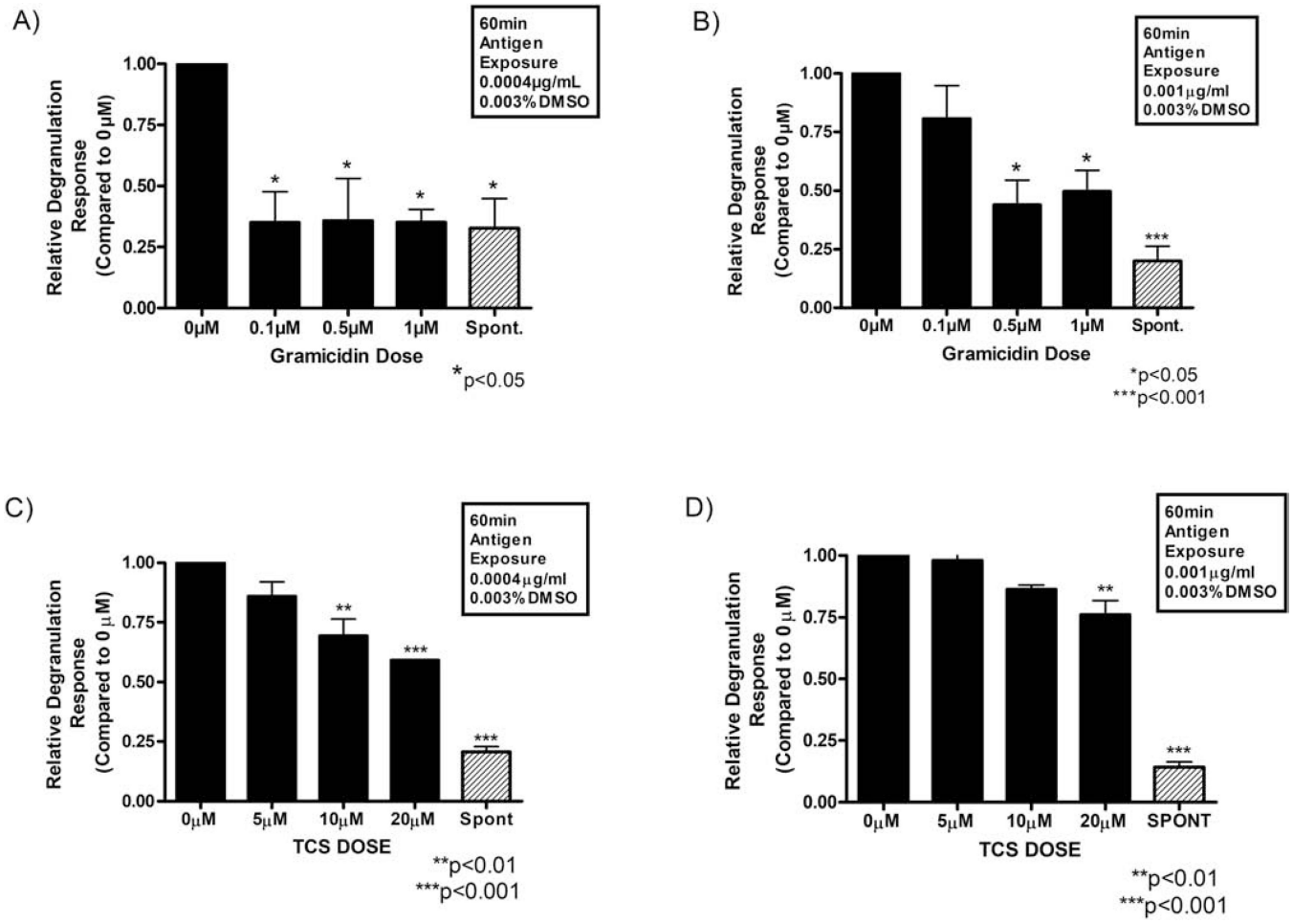


**Figure 2.**

Relative degranulation response of antigen-stimulated RBL mast cells exposed to micromolar doses of the canonical plasma membrane depolarizer gramicidin (**A** and **B**) or to triclosan (**C** and **D**). IgE-sensitized cells were stimulated for 1 h with either 0.0004 μg $mL^{-1}$ Ag (**A** and **C**) or 0.001 μg $mL^{-1}$ Ag (**B** and **D**). All samples (**A** - **D**) contained 0.003% DMSO, which was the vehicle required for gramicidin dissolution. For spontaneous release ("Spont" on x-axes), cells were incubated for 1 h in BT with 0.003% DMSO (with no IgE, Ag, TCS, or gramicidin). Values represent the mean ± SEM of 3 independent experiments; three replicates per treatment type were used each experimental day. Statistically significant results, as compared to the appropriate control (0 μM TCS + DMSO vehicle) or (0 μM gramicidin + DMSO vehicle), are represented by *p < 0.05, **p < 0.01, ***p<0.001 as determined by one-way ANOVA followed by Tukey's post-hoc test.

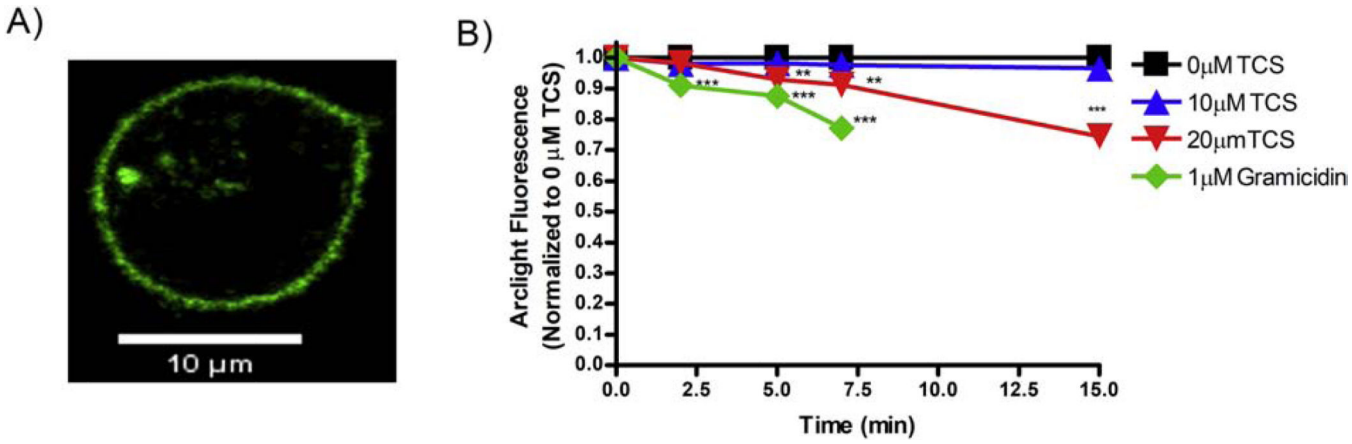


**Figure 3.**

Triclosan and gramicidin effects on fluorescence of ArcLight-A242 in RBL mast cells. (**A**) One representative live-cell confocal microscopy image of an RBL mast cell transiently transfected with ArcLight construct, prior to gramicidin or TCS treatment. Scale bar, 10 µm. (**B**) RBL cells were transiently transfected with ArcLight, washed with BT, exposed to control (BT) (N = 52), 10 µM TCS (N = 22), 20 µM TCS (N = 28), or 1 µM gramicidin (N = 24) for 15 minutes. At each time point, the average fluorescence of each plasma membrane was measured, background-subtracted, and normalized to the 0 min timepoint, as described in Methods. Values presented are means ± SEM of at least 3 independent days of experiments per treatment. Statistically significant results at each timepoint, as compared to the appropriate control (0 µM TCS or 0 µM gramicidin + DMSO vehicle), are represented by **$p < 0.01$, ***$p < 0.001$, as determined by one-way ANOVA followed by Tukey's post-hoc test.

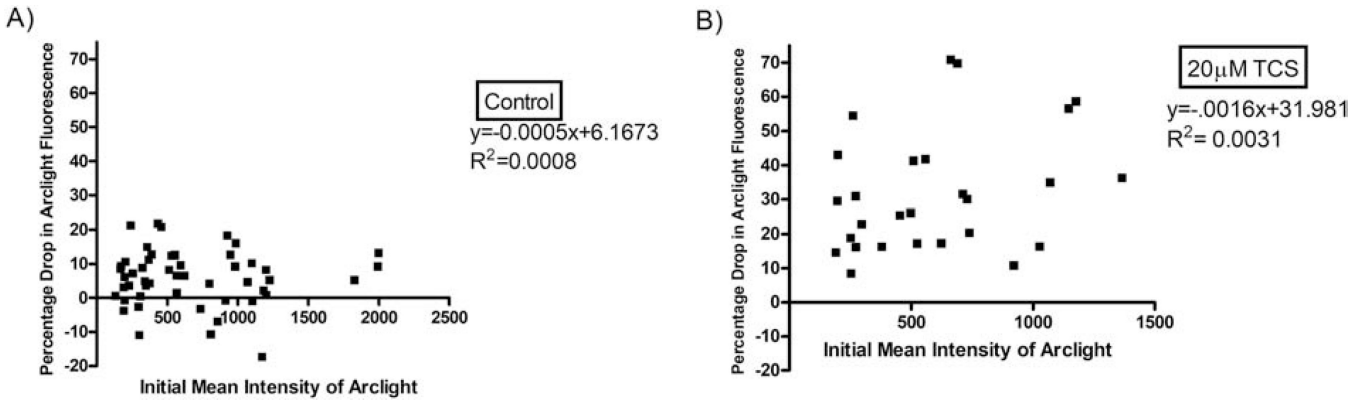


**Figure 4.**

Effect of cellular expression level of ArcLight-A242 on TCS inhibition of ArcLight-A242 fluorescence. Data from Figure 3B, ArcLight-A242 transfected cells analyzed by confocal imaging and image analysis comparing control (0μM TCS) and 20μM TCS treatments, were plotted as individual cells' data. The percentage drop in fluorescence by 15 minutes time of exposure, for each individual cell, is plotted as a function of that cell's initial mean intensity of ArcLight-A242. Statistical results per plot are represented by equation of linear regression and $R^2$ values.

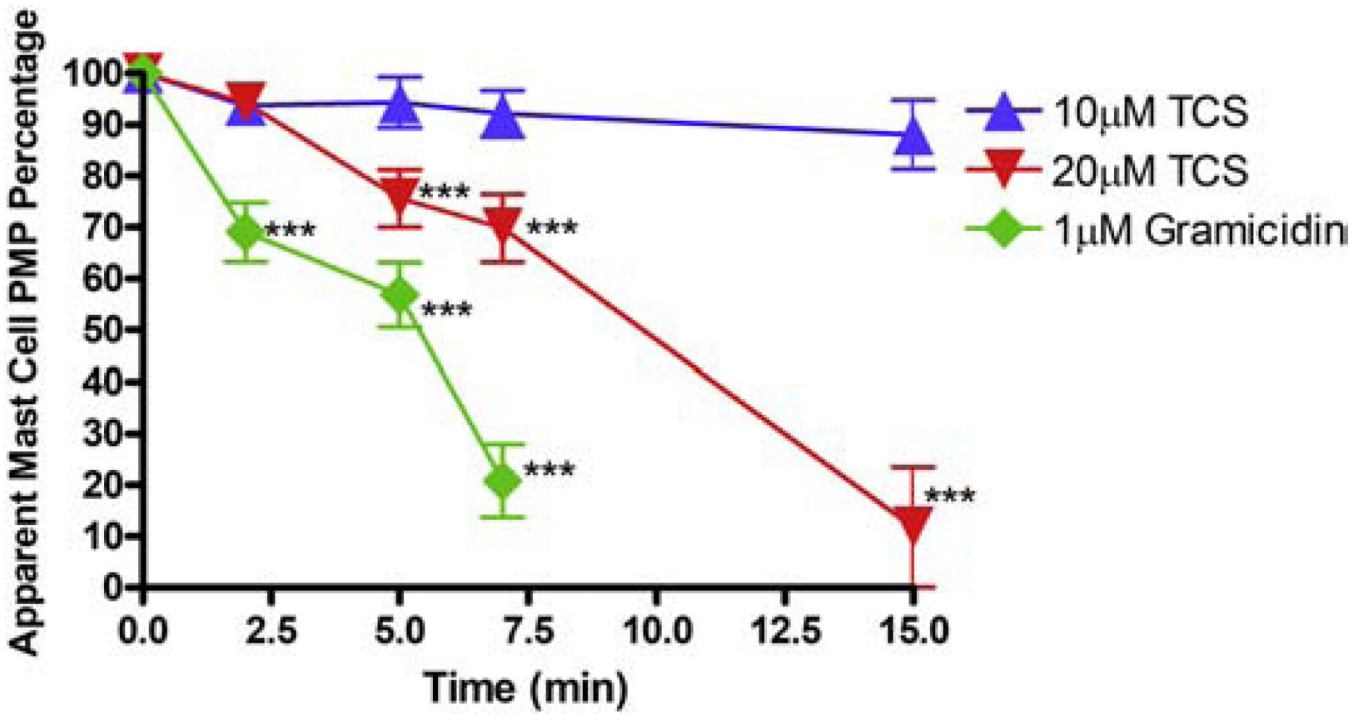


**Figure 5.**

Triclosan and gramicidin apparent effects on plasma membrane potential (PMP) of RBL mast cells. Data from Figure 3B were utilized to calculate percentage of PMP (with each 0 min timepoint defined as 100%) as a function of time (min), as described in Methods. Values presented are means ± SEM of at least 3 independent days of experiments per treatment. Statistically significant results at each timepoint, as compared to the appropriate control (0 μM TCS or 0 μM gramicidin + DMSO vehicle), are represented by ***$p < 0.001$, as determined by one-way ANOVA followed by Tukey's post-hoc test.

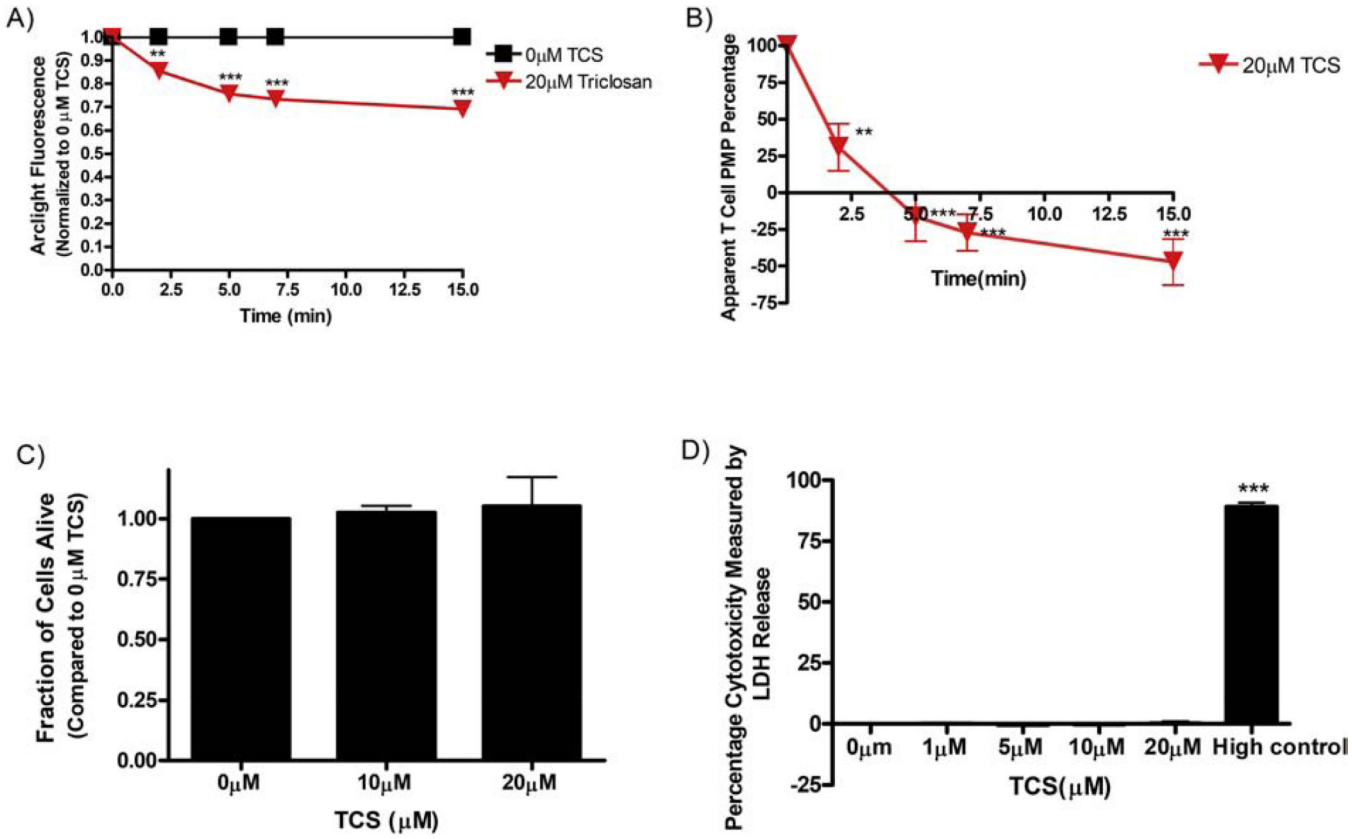


**Figure 6.**

Triclosan effects on fluorescence of ArcLight-A242 in human Jurkat T cells, triclosan apparent effects on Jurkat plasma membrane potential (PMP), and cytotoxicity determination. **(A)** Jurkat cells were transiently transfected with ArcLight-A242, washed with BT, exposed to BT (0 μM TCS) (N=20) or 20 μM TCS (N=17) for 15 minutes. At each time point, the average fluorescence of each plasma membrane was measured, background-subtracted, and normalized to the 0 min timepoint, as described in Methods. **(B)** Data from Figure 6A were utilized to calculate percentage of PMP (with each 0 min timepoint defined as 100%) as a function of time (min), as described in Methods. **(C)** Jurkat T cell cytotoxicity to TCS was assessed by trypan-blue exclusion assay and by **(D)** lactate dehydrogenase (LDH) detection kit from Roche. “High control” is a sample treated with lysis solution provided by the kit. Values presented are mean ± SEM of at least three independent experiments. Statistically significant results, as compared to appropriate control, are represented by **p<0.01, ***$p < 0.001$, as determined by one-way ANOVA followed by Tukey’s *post-hoc* test.

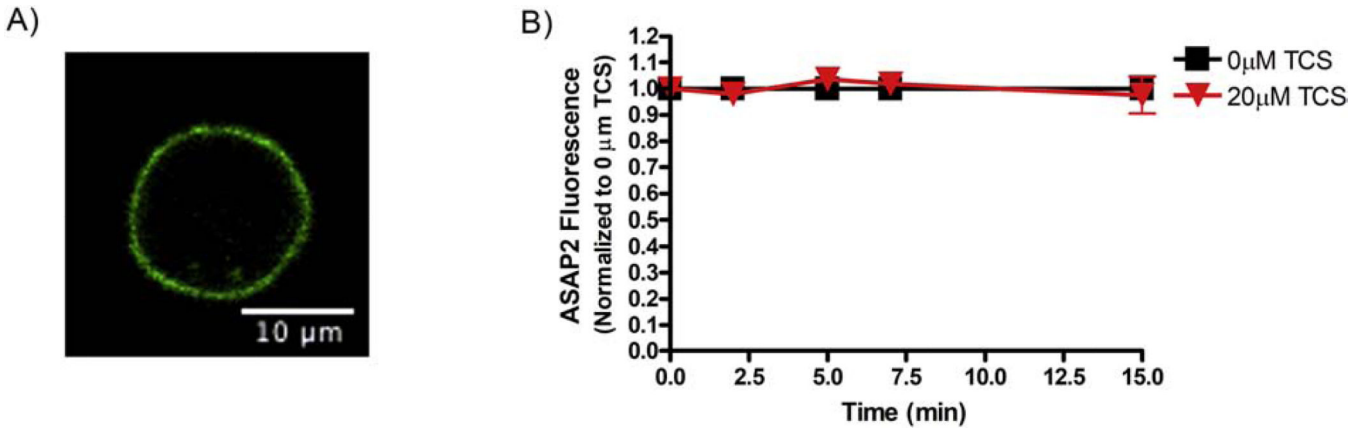


**Figure 7.**

Triclosan effects on fluorescence of ASAP2 in RBL mast cells. (**A**) One representative live-cell confocal microscopy image of an RBL mast cell transiently transfected with ASAP2 construct, prior to TCS treatment. Scale bar, 10 µm. (**B**) RBL cells were transiently transfected with ASAP2, washed with BT, exposed to control (BT) (N=18) or 20 µM TCS (N=21) for 15 minutes. At each time point, the average fluorescence of each plasma membrane was measured, background-subtracted, and normalized to the 0 min timepoint, as described in Methods. Values presented are means ± SEM of at least 6 independent experiments per treatment. Analysis by one-way ANOVA followed by Tukey's post-hoc test found no statistical significance.

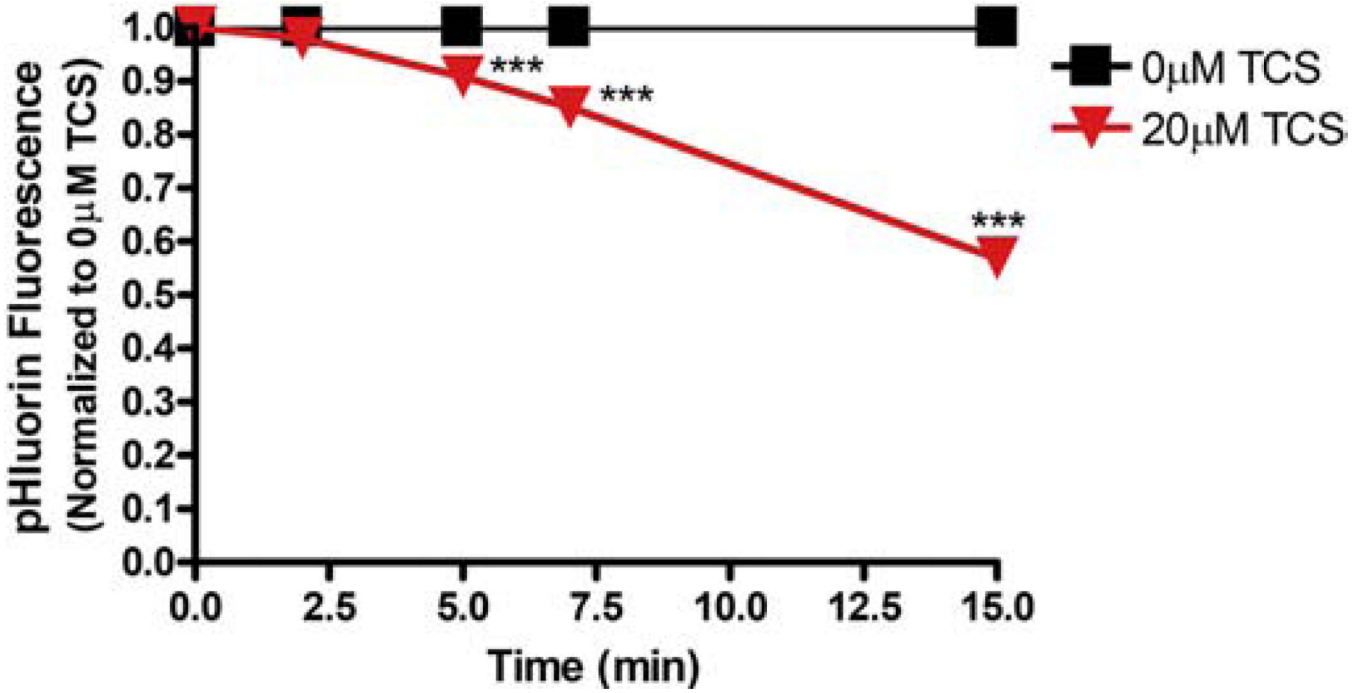


**Figure 8.**

Triclosan effects on fluorescence of Lyn-tailed mCherry-SuperEcliptic (SE) pHluorin in RBL mast cells. RBL cells were transiently transfected with Lyn-tailed mCherry-SE pHluorin, washed with BT, and exposed to BT (N=35) or 20 μM TCS (N=52) for 15 minutes. At each time point, the average fluorescence of each plasma membrane was measured, background-subtracted, and normalized to the 0 min timepoint, as described in Image J Automated Methods. Values presented are means ± SEM of 3 independent days of experiments per treatment. Statistically significant results at each timepoint, as compared to the appropriate control (0 μM TCS or 0 μM gramicidin + DMSO vehicle), are represented by ***$p < 0.001$, as determined by one-way ANOVA followed by Tukey's post-hoc test.

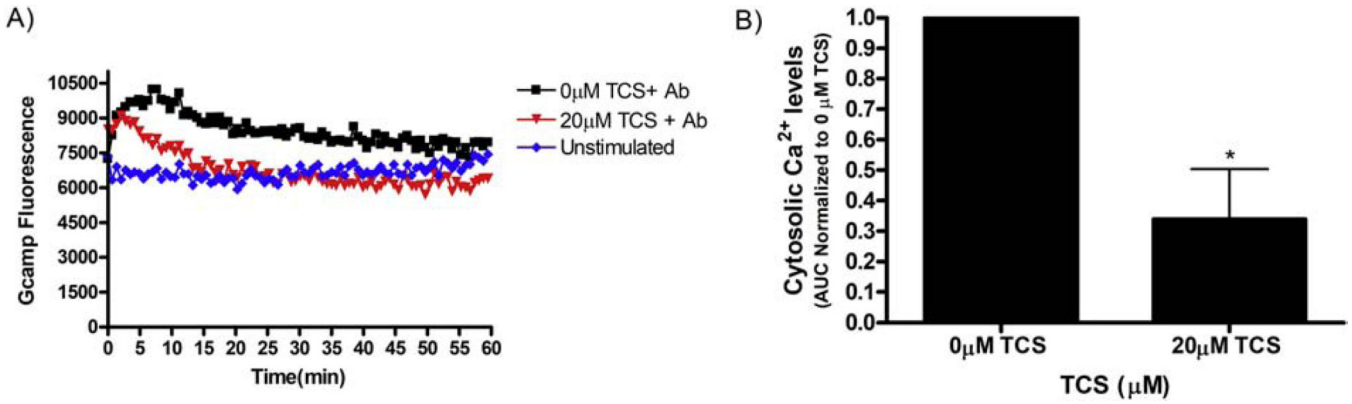


**Figure 9.**

Triclosan effects on cytosolic $Ca^{2+}$ levels as activated by anti-T Cell Receptor (TCR) antibody in Jurkat T Cells. Jurkat cells were transiently transfected with cytosolic Gcamp6 overnight, then exposed in BT Control or 20 μM TCS, each with 0.2 μg/ml anti-TCR ("Ab") for 1 hour. "Unstimulated" contained no TCS and no anti-TCR. Raw fluorescence was measured using a microplate reader as described in Methods. **(A)** Representative figure (no error bars) shows fluorescence obtained following background fluorescence subtraction (mock-transfected cells' fluorescence) from treatment groups at each time point. **(B)** Area under the curve (AUC) was obtained from the fluorescence curves and values were normalized to the control of each day for 3 replicates per treatment group per day. AUC values presented are means ± SEM of 3 independent days of experiments. Statistically significant results, as compared to the appropriate control (0μM TCS), are represented by *$p < 0.05$, as determined by unpaired t-test.

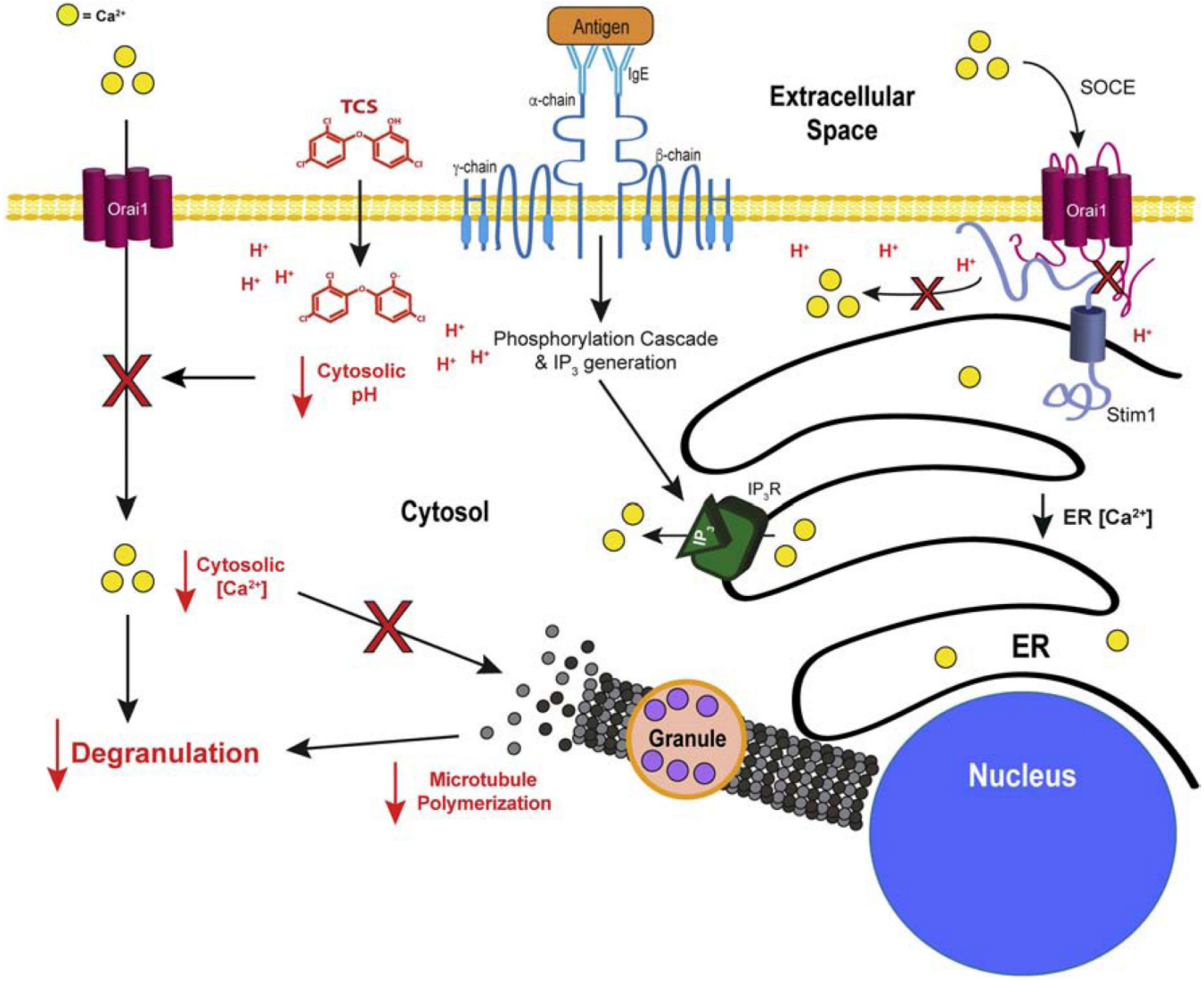


**Figure 10.**

Effects of triclosan on mast cell signaling. Antigen crosslinking of IgE receptors, early phosphorylation events, and calcium release from the ER are uninhibited by TCS. However, TCS brings protons into the cytosol, decreasing cytosolic pH, thereby inhibiting CRAC channel activation, cytosolic calcium levels, microtubule polymerization, and, subsequently, degranulation.

**Table 1.**

Summary of estimated changes in cytosolic pH following TCS exposure.

| Method | Magnitude of pH Change | Citation |
|---|---|---|
| Calculated estimate | −0.3 | Discussion |
| ArcLight experiments | −0.23 | Figure 3 |
| pHlourin experiments | −0.37 | Figure 8 |
| Average | −0.3 | Table 1 |